

Higgs studies in polarized $\gamma\gamma$ collisions

V.S. Fadin^{1,2}, V.A. Khoze^{1,3} and A.D. Martin¹

- ¹ Department of Physics, University of Durham, Durham, DH1 3LE, UK.
- ² Budker Institute for Nuclear Physics and Novosibirsk State University, 630090 Novosibirsk, Russia.
- ³ INFN - Laboratori Nazionali di Frascati, PO Box 13, 00044, Frascati, Italy.

Abstract

The study of an intermediate mass Higgs boson, via the process $\gamma\gamma \rightarrow H \rightarrow b\bar{b}$ from an initially polarized $J_z = 0$ state, has been advocated as an important feasible goal of a future photon linear collider. The crucial argument was the m_b^2/s suppression of the background process $\gamma\gamma(J_z = 0) \rightarrow b\bar{b}$. We critically review the contribution of the radiative background processes (in which the m_b^2/s suppression is absent) to the quasi-two-jet-like events with at least one, but preferably two, tagged energetic b jets. Within a complete study of the radiative processes, we find that a sizeable background contribution can come from the helicity-violating $\gamma\gamma(J_z = 0) \rightarrow b\bar{b}$ process accompanied by soft gluon emission. These latter radiative corrections contain a new type of double logarithmic (DL) terms. We clarify the physical nature of these novel DL corrections. Despite the fact that the one-loop DL terms are comparable or even larger than the Born term, fortunately we find that the calculation of the cross section in the two-loop approximation is sufficient for a reliable evaluation of the background to the Higgs signal.

1. Introduction

Now that the top quark has been discovered, the Higgs particle H is the only fundamental object of the Standard Model which has not been found experimentally. Many theoretical studies have been performed (see, for example, reviews [1]-[6]) in order to examine various aspects of Higgs hunting. Searches in the near future are concentrating on the possibility of finding a Higgs boson in the so-called intermediate mass region,

$$65 \lesssim M_H \lesssim 140 \text{ GeV}. \quad (1)$$

Within the Standard Model such a Higgs particle decays dominantly into a $b\bar{b}$ pair with the decay coupling being proportional to the b -quark mass m_b .

In this connection it is relevant to note that various fundamental physics issues could be examined in the collisions of high-brightness, high-energy photon beams at future linear colliders (see e.g. [7]-[9]). In fact the rapid advances of laser technology make possible just such a new type of experimental facility known as a Photon Linear Collider or PLC [10]-[11] in which high energy photon beams are produced by the Compton back-scattering of laser photons off linac electrons.

One particularly interesting use of the PLC would be to measure the two-photon decay width of a Higgs boson once it is discovered [12, 13]. The $\gamma\gamma$ width of H is one of its most important properties. The coupling of the Higgs to two photons proceeds through a sum of loop diagrams for all charged particles which couple to the Higgs. For example, the decay width $\Gamma(H \rightarrow \gamma\gamma)$ can explore the possible existence of quarks heavier than the top since they contribute without being suppressed by their large mass. Therefore this channel may provide a way to count the number of such heavy quarks.

In a PLC, the partial width $\Gamma(H \rightarrow \gamma\gamma)$ is deduced by measuring the Higgs production cross section in the reaction

$$\gamma\gamma \rightarrow H \rightarrow b\bar{b}. \quad (2)$$

The number of detected events is proportional to the product $\Gamma(H \rightarrow \gamma\gamma) B(H \rightarrow b\bar{b})$. Thus, a measurement of the $b\bar{b}$ production cross section can, in principle, determine this product. An independent measurement of the branching ratio $B(H \rightarrow b\bar{b})$, say at an e^+e^- collider in the process $e^+e^- \rightarrow ZH \rightarrow ZX$ [14, 15], then allows a determination of the $\gamma\gamma$ partial width. However, to isolate $b\bar{b}$ production induced by an intermediate mass Higgs boson we must first suppress the continuum

$$\gamma\gamma \rightarrow q\bar{q} \quad (\text{with } q = b, c) \quad (3)$$

background events which lie beneath the resonant signal ($\gamma\gamma \rightarrow H \rightarrow b\bar{b}$), assuming that the b and c quarks can be distinguished from light quarks by tagging of at least one heavy quark jet.

In order to suppress the continuum background it has been proposed [12, 13] that we exploit¹ the polarisation dependence of the $\gamma\gamma \rightarrow q\bar{q}$ cross sections (e.g. [16, 17]). Recall that the Higgs

¹We assume that it is experimentally possible to separate $J_z = 0$ and $|J_z| = 2$ $\gamma\gamma$ beams. The z axis is taken along one of the incoming photon beam directions. According to the present understanding it appears feasible to achieve a polarisation ratio $P = (J_z = 0)/(|J_z| = 2)$ of 20–50 at a PLC [11, 13].

signal is produced from a $\gamma\gamma$ initial state with $J_z = 0$. The idea is that the background is dominantly produced from a $J_z = \pm 2$ initial state, whereas the $J_z = 0$ (Born) cross section is suppressed for large angle q and \bar{q} production by a factor of m_q^2/s [12, 16, 18].

The physical origin of this suppression [9, 18] is related to the symmetry properties of the helicity amplitudes $M_{\lambda_1, \lambda_2}^{h, \bar{h}}$ describing the background process

$$\gamma(\lambda_1, k_1) + \gamma(\lambda_2, k_2) \rightarrow q(h, p) + \bar{q}(\bar{h}, \bar{p}). \quad (4)$$

Here λ_i are the helicities of the incoming photons, and h and \bar{h} are the (doubled) helicities of the produced quark and antiquark. The k 's and p 's denote the particle four-momenta. It can be shown, using an analogous argument to that in [18], that the real part of the amplitude for a $J_z = 0$ initial state ($\lambda_1 = \lambda_2$) and the opposite helicities of the quark and antiquark ($\bar{h} = -h$) vanishes in all orders in perturbative theory, that is

$$\text{Re } M_{\lambda, \lambda}^{h, -h} = 0. \quad (5)$$

If we take into account quark helicity conservation, then for large angle production we also have

$$M_{\lambda, \lambda}^{h, h} \sim \mathcal{O}\left(\frac{m_q}{\sqrt{s}}\right) M_{\lambda, -\lambda}^{h, -h}, \quad (6)$$

where the amplitude on the right-hand-side displays the dominant helicity configuration of the background process at large angles. The above-mentioned m_q^2 suppression of the $J_z = 0$ Born cross section is a consequence of Eqs. (5) and (6) and the fact that the Born amplitudes are real. Note that we are only concerned with background $\gamma\gamma \rightarrow q\bar{q}$ production at large angles since this is the event topology of the Higgs signal². Here and in what follows we will take the $\gamma\gamma$ centre-of-mass collision energy $\sqrt{s} = M_H$.

In the Born approximation the straightforward calculation of the above $J_z = 0$ amplitudes gives

$$\left(M_{\lambda, \lambda}^{h, \bar{h}}\right)_{\text{Born}} = \frac{8\pi \alpha Q_q^2}{(1 - \beta^2 \cos^2 \theta)} \frac{2m_q}{\sqrt{s}} (\lambda + \beta h) \delta_{h, \bar{h}}, \quad (7)$$

where $\beta \equiv \sqrt{1 - 4m_q^2/s}$, and m_q and Q_q are the mass and electric charge of the quark respectively. Thus we see that in the Born approximation $\gamma\gamma \rightarrow q\bar{q}$ production in the $J_z = 0$ channel is suppressed³ by a factor m_q^2/M_H^2 . That is for at energies $\sqrt{s} \approx M_H$

$$d\sigma^{\text{Born}}(J_z = 0) \sim \frac{m_q^2}{M_H^2} d\sigma^{\text{Born}}(J_z = \pm 2) \quad (8)$$

²Here we require that most of the $\gamma\gamma$ collision energy is deposited in the central detector. This provides a very strong suppression of the resolved photon contributions, such as $\gamma \rightarrow gX$, followed by $g\gamma \rightarrow q\bar{q}$ [18, 20]. Such processes will therefore not be considered here.

³We see that in the high energy limit the $J_z = 0$ amplitude is additionally m_q -suppressed when $\lambda = -h$. This suppression is readily seen in the results of ref. [16].

with the $J_z = \pm 2$ cross section having the normal behaviour

$$d\sigma^{\text{Born}}(J_z = \pm 2) \sim \frac{\alpha^2}{M_H^2}. \quad (9)$$

So far so good — in the $J_z = 0$ $\gamma\gamma$ channel the $b\bar{b}$ ($c\bar{c}$) background process appears to be suppressed by a large factor, m_q^2/M_H^2 . However, we must consider contributions beyond the Born approximation.

First, we note that the amplitude $M_{\lambda,\lambda}^{h,-h}$ acquires an imaginary part related to discontinuities of diagrams of the type shown in Fig. 1. The corresponding $\mathcal{O}(\alpha_S^2)$ contribution to the $\gamma\gamma \rightarrow q\bar{q}$ cross section, $d\sigma^{\text{Im}}$, is non-zero⁴ in the $m_q = 0$ limit. In fact, at very high energies this contribution dominates large angle $q\bar{q}$ production from the $J_z = 0$ initial state. However, an explicit calculation [21] shows (in the central region, $\theta \sim 1$, and for energy $\sqrt{s} = M_H \sim 100$ GeV) that $d\sigma^{\text{Im}}(J_z = 0)$ is at least an order of magnitude smaller than the Born approximation result. The ratio reaches its maximum at $\theta = \pi/4$ where

$$\left(\frac{d\sigma^{\text{Im}}(J_z = 0)}{d\sigma^{\text{Born}}(J_z = 0)} \right)_{\text{max}} \simeq \frac{2}{9} \frac{\alpha_S^2(M_H^2)}{\pi^2} \frac{M_H^2}{m_b^2} \lesssim 0.1, \quad (10)$$

for $M_H \approx 100$ GeV. We therefore neglect the $d\sigma^{\text{Im}}$ contribution from now on.

More seriously, the m_q^2/M_H^2 suppression of the $J_z = 0$ $\gamma\gamma \rightarrow q\bar{q}$ background is, in principle, removed by gluon bremsstrahlung in the final state [18]⁵. In other words the radiative process $\gamma\gamma \rightarrow q\bar{q}g$ (with $q = b, c$) can have a dramatic effect. It can mimic the $b\bar{b}$ two-jet topology of the Higgs signal in two important ways: (i) if partons are quasi-collinear, for example, a fast quark recoiling against a collinear quark and gluon, or (ii) if one of the partons is either quite soft or is directed down the beampipe and is therefore not tagged as a distinct jet. A particularly interesting example [18] of the latter is when one of the incoming photons splits into a quark and an antiquark, one of which carries most of the photon's momentum and Compton scatters off the other photon, $q(\bar{q})\gamma \rightarrow q(\bar{q})g$ (see Fig. 2). Two jets are then identified in the detector, with the third jet remaining undetected.

In the ideal situation in which we clearly identify two narrow b quark jets, the radiative background is not a problem. However, in the realistic experimental situation the isolation of the Higgs signal will be much more problematic. To reduce the (radiative) background it will be necessary to perform a detailed study of the optimum jet shape cuts and to consider the efficiency of the separation of b jets from c jets (see, for example, [13, 18, 19]). In fact distinguishing b from c jets will be a crucial experimental task. We note the factor of 16 amplification of $\gamma\gamma \rightarrow c\bar{c}$ over $\gamma\gamma \rightarrow b\bar{b}$ due to the different charges of the quarks.

Our main concern here is the calculation of the radiative corrections to the background process $\gamma\gamma \rightarrow q\bar{q}$, which is found to have several interesting features in its own right. We begin

⁴It vanishes in the special case of scattering at $\theta = 90^\circ$ [9, 18].

⁵The impact of the radiative background processes on the phenomenology of an intermediate mass Higgs boson at PLC has also been studied in the recent papers [20]-[23].

our study with a brief review of how the radiative 3 jet process, $\gamma\gamma \rightarrow q\bar{q}g$, can mimic the Higgs $\gamma\gamma \rightarrow H \rightarrow b\bar{b}$ signal in the so-called collinear and Compton configurations. In Section 3 we extend the existing evaluation of the Compton contribution to the case of polarised photons using the method of quasi-real fermions. We then turn from radiative to non-radiative corrections. In Section 4 we clarify the physical origin of the novel non-Sudakov double logarithmic (DL) terms which occur in helicity-violating amplitudes. The DL terms look particularly dangerous for $\gamma\gamma \rightarrow q\bar{q}$ amplitudes with equal photon helicities because of the large coefficient at the one-loop level (namely $c_1 = -8$ in (21) and (64)). To investigate their total potential effect we therefore, in Section 5, calculate the DL contribution at the two-loop level. Fortunately, we find that this is sufficient to provide a reliable evaluation of the non-radiative corrections. We explain the physical reason why this is so. In Section 6 we finish with a short discussion of the impact of radiative corrections on the background to the Higgs signal that can be produced in polarised photon-photon collisions.

2. Overview of radiative corrections

The non-radiative backgrounds of the Higgs signal in $\gamma\gamma$ collisions were considered in [13]. With highly polarized photon beams, such backgrounds were believed to be small and hence thought not to hinder the study of an intermediate-mass Higgs boson at a $\gamma\gamma$ collider. For example, if the resolution for reconstructing the Higgs mass M_H is 10 GeV then in the Born approximation the ratio R of the signal to background $b\bar{b}$ events in the $J_z = 0$ channel is

$$R \sim \left(\frac{M_H}{60 \text{ GeV}} \right)^5. \quad (11)$$

This estimate applies if the Higgs lies in the 65–120 GeV mass interval, see Refs. [13, 18].

The analysis of [13] was based only on Born level calculations of $b\bar{b}$ (and $c\bar{c}$) production. However, more recently it has been pointed out [18]–[23] that QCD corrections are very important and considerably complicate the extraction of the Higgs signal from the background. The problem is evident once we note that the cross section for the radiative background process $\gamma\gamma \rightarrow q\bar{q}g$, unlike the Born signal of (8), does not contain the m_q^2/M_H^2 suppression factor.

The aim of this paper is to systematically study the QCD radiative corrections to $\gamma\gamma \rightarrow q\bar{q}$ in the $J_z = 0$ channel. Before we present detailed calculations it is informative to give order-of-magnitude estimates of the relevant processes. We have to consider corrections to the two-body $b\bar{b}$ (or $c\bar{c}$) final state, as well as studying the impact of radiative $q\bar{q}g$ production. As mentioned above, the latter is a particular problem for the $\gamma\gamma \rightarrow H \rightarrow b\bar{b}$ jet signal in two different kinematic regimes: the collinear and Compton configurations.

By the collinear configuration we mean the production of the q and \bar{q} at large angles accompanied by gluon radiation with limited maximal energy ΔE_g in the direction orthogonal to the most energetic quark. This applies in the region

$$\frac{m_q}{M_H} < \varepsilon_g \ll 1, \quad (12)$$

where $\varepsilon_g = \Delta E_g/M_H$. Then we have

$$\sigma(\gamma\gamma|_{J_z=0} \rightarrow q\bar{q}g) \sim \frac{\alpha^2 Q_q^4}{M_H^2} \frac{\alpha_S(\varepsilon_g M_H)}{\pi} \varepsilon_g \ln \frac{1}{\varepsilon_g}, \quad (13)$$

which manifestly does not contain the factor m_q^2/M_H^2 , but which can be suppressed by taking ε_g small. If the acollinearity of the q and \bar{q} jets were allowed to be large such that $\varepsilon_g \sim \mathcal{O}(1)$ then the radiative background becomes

$$\sigma(\gamma\gamma|_{J_z=0} \rightarrow q\bar{q}g \rightarrow 3 \text{ jets}) \sim \sigma(\gamma\gamma|_{J_z=\pm 2} \rightarrow q\bar{q}g \rightarrow 3 \text{ jets}) \sim \frac{\alpha^2 Q_q^4}{M_H^2} \frac{\alpha_S(M_H)}{\pi} \quad (14)$$

which greatly exceeds the Higgs signal — so clearly this is not a regime in which to search for the Higgs boson.

The Compton configuration of the $q\bar{q}g$ background is shown in Fig. 2. In this case it is the outgoing quark (or antiquark) along the photon beam direction ε_q which is comparatively soft, that is

$$\frac{m_q}{M_H} < \varepsilon_q \ll 1, \quad (15)$$

where $\Delta E_q = \varepsilon_q M_H$ is its maximal allowed quark energy. The cross section is of the form

$$\sigma(\gamma\gamma|_{J_z=0,\pm 2} \rightarrow q\bar{q}g)_{\text{Compton}} \sim \frac{\alpha^2 Q_q^4}{M_H^2} \frac{\alpha_S(M_H)}{\pi} \varepsilon_q \ln \frac{\varepsilon_q M_H}{m_q}, \quad (16)$$

where the logarithm arises from the integration over the transverse momentum of the spectator quark. Incidentally, to separate the dominant contribution (16) arising from one energetic and one comparatively soft b quark from the Higgs topology with two fast b quarks may pose an experimental challenge, see Ref. [18] for details.

In summary, to have a chance to isolate the Higgs contribution we require the observation of two energetic (b, \bar{b}) jets with at least one, and preferably two, tagged b quarks. To reduce the radiative $q\bar{q}g$ background we must impose kinematic cuts, such as $\varepsilon_g, \varepsilon_q \ll 1$. However, there is a price to pay, since the signal is also depleted. Indeed

$$\sigma(\gamma\gamma \rightarrow H \rightarrow b\bar{b} \text{ jets}) = \tilde{\sigma}(\gamma\gamma \rightarrow H \rightarrow b\bar{b}) F_g. \quad (17)$$

where F_g is a Sudakov form factor [24] which occurs because we need to impose a cut (say $\varepsilon_g \ll 1$) in order to prohibit energetic gluon emissions. F_g involves a resummation of double logarithmic terms. Its explicit form depends on the cut-off conditions on the accompanying gluon radiation, see for details the end of section 4. Thus when imposing the restriction (12) we need to resum the $(\alpha_S L_g^2)^n$ terms where

$$L_g \equiv \ln \left(\frac{1}{\varepsilon_g} \right). \quad (18)$$

If, on the other hand, the gluon energy is restricted, $k_{\max} = k_0$, then a resummation of DL terms of the form $(\alpha_S L_m L_0)^2$ is required. Here

$$L_m \equiv \ln \left(\frac{M_H}{m_q} \right), \quad L_0 \equiv \ln \frac{M_H}{k_0}. \quad (19)$$

The form factor decreases rapidly if ε_g (or k_0) is taken to be smaller. That is the more we require the b and \bar{b} jets to be collinear then the more we reduce the signal. The second effect, which introduces $\tilde{\sigma}$ in (17), is due to higher order (single logarithmic, $\alpha_S L_m$) QCD effects which are known [25]–[27] to diminish the corresponding Born result by a factor of approximately two. The reduction arises from running the b quark mass from $\overline{m}_b(m_b)$ up to its value $\overline{m}_b(M_H)$ at the Higgs scale. Here $\overline{m}_b(\mu)$ is the running b quark mass in the $\overline{\text{MS}}$ scheme [28].

We may write the cross section for the background arising from the central production of quasi-two-jet-like events with at least one energetic b jet tagged in the form

$$\begin{aligned} \sigma(\gamma\gamma|_{J_z=0} \rightarrow 2 \text{ jets})_{\text{single } b \text{ tag}} &= \sigma(\gamma\gamma|_{J_z=0} \rightarrow b\bar{b}) F_g F_q + \sigma(\gamma\gamma|_{J_z=0} \rightarrow b\bar{b}g \rightarrow 2 \text{ jets})_{\text{collinear}} \\ &+ \sigma(\gamma\gamma|_{J_z=0} \rightarrow b\bar{b}g \rightarrow 2 \text{ jets})_{\text{Compton}}. \end{aligned} \quad (20)$$

This formula displays the general structure of the background contributions.⁶ The first term contains a new non-Sudakov form factor F_q which arises from virtual diagrams of the type shown in Fig. 1. The physical origin of this form factor is elucidated in section 4. In the double logarithmic (DL) approximation F_q has the form

$$F_q(L_m) = \sum_n c_n \left(\frac{\alpha_S}{\pi} L_m^2 \right)^n \quad (21)$$

with $c_0 = 1$ and $c_1 = -8$ [21] so that the second negative term in (21) dominates over the Born term for $M_H \sim 100$ GeV. This dominance undermines the results of analyses [20]–[23] which are based on the one-loop approximation. The calculation of the coefficient c_2 is one of the aims of the present work, see section 5. It is worth noting that the same form factor F_q occurs in the signal (17) and in the background contribution (20). Note from (11) that the non-radiative $J_z = 0$ background, the first term in (20), is most important for the smaller Higgs masses in the interval given in (1).

The collinear contribution in (20), in which we have gluon bremsstrahlung off one of the energetic b quarks, can be suppressed by using the ε_g cut, see Eq. (13), (or the traditional y_{cut}) to discriminate between two and three jet topologies [18]. However, we note here, that due to the form factor F_g , the imposition of the cut-off will automatically deplete the signal (as well as the first term in (20)). It could be a non trivial task to find the optimal choice for the cut-off.

⁶Note that without a thorough study of the single logarithmic effects, the question concerning the b -quark mass prescription in the first term in (20) remains open.

As we have seen in (16) the Compton contribution is sizeable and should be avoided if at all possible by tagging energetic b and \bar{b} jets. Obviously such double tag events have no contribution from the Compton configuration. The Compton contribution was roughly estimated in [18] by exploiting the fact that it does not have a particularly strong dependence on the helicities of the photons. Since the Compton regime may play an important role in realistic experiments we calculate the cross section to logarithmic accuracy in the next section.

3. The Compton regime contribution

As we mentioned above, in the case when only one b jet is identified the $\gamma\gamma \rightarrow b\bar{b}g \rightarrow 2$ jet cross section may receive a large contribution from the configuration where the energetic quark and gluon appear as jets in the central detector and the spectator quark is comparatively soft and quasi-collinear with one of the incoming photons (the so-called Compton regime [18]). The size of the virtual Compton scattering contribution was qualitatively estimated in [18] for the case of unpolarized photons.

For polarized photons we use the method of “quasi-real fermions” [29] to evaluate the Compton contribution of Fig. 2 in the region where the maximal energy of the unregistered quark satisfies

$$\Delta E_q = \varepsilon_q M_H \gg m_q. \quad (22)$$

This enables us to write, to logarithmic accuracy, the matrix element in the factorized form

$$\begin{aligned} M\left(\gamma(\lambda_1, k_1) + \gamma(\lambda_2, k_2) \rightarrow q(h, p) + \bar{q}(\bar{h}, \bar{p}) + g(\lambda_g, k)\right)_{\text{Compton regime}} \\ = \sum_{h'} f_{\lambda_1}^{h'\bar{h}} \cdot \overline{M}_{\text{Compton}}\left(\gamma(\lambda_2, k_2) + q(h', k_1 - \bar{p}) \rightarrow q(h, p) + g(\lambda_g, k)\right), \end{aligned} \quad (23)$$

where the helicities (λ or $\frac{1}{2}h$) and four momenta of the various particles are indicated in brackets. The amplitude f , which describes the $\gamma(\lambda_1) \rightarrow q(h') \bar{q}(\bar{h})$ splitting, is given by

$$f_{\lambda_1}^{h'\bar{h}} = -\frac{e Q_q}{2(k_1 \cdot \bar{p})} \bar{u}^{h'}(k_1 - \bar{p}) \not{\epsilon}_{\lambda_1}(k_1) v^{\bar{h}}(\bar{p}), \quad (24)$$

where $\not{\epsilon} \equiv \gamma \cdot e$ and e^μ is the polarization vector of the photon. We normalise the four component helicity spinors so that

$$(u^h)^\dagger u^h = 2p_0, \quad (v^{\bar{h}})^\dagger v^{\bar{h}} = 2\bar{p}_0. \quad (25)$$

The amplitude $\overline{M}_{\text{Compton}}$, which describes the hard Compton subprocess, is evaluated on-mass-shell and all quark masses are neglected. The other three contributions corresponding to the interchanges $q \leftrightarrow \bar{q}$ and/or $k_1 \leftrightarrow k_2$ in Fig. 2 are obtained from (23) and (24) by the obvious substitutions.

We denote the (unnormalized) polarization density matrix of the incoming quark in the Compton subprocess by $\bar{\rho}$. That is

$$\bar{\rho}^{h'h''} = \sum_{\bar{h}} f_{\lambda_1}^{h'\bar{h}} (f_{\lambda_1}^{h''\bar{h}})^*, \quad (26)$$

where for clarity we have omitted the λ_1 subscript.

Now in the ultrarelativistic limit for small angles $\bar{\theta}$ of the outgoing spectator antiquark with respect to the parent photon direction \mathbf{k}_1 we find (24) gives

$$\begin{aligned} \frac{\bar{p}^{h'h''}}{\bar{p}_{\lambda_1}} &\simeq \frac{\pi\alpha Q_q^2}{(k_1 \cdot \bar{p})^2} \omega^2 \left(\frac{\bar{x}}{1-\bar{x}} \right) \\ &\left\{ \left[\bar{\theta}^2 \left((1-\bar{x})^2 + \bar{x}^2 + \lambda_1 h'(1-2\bar{x}) \right) + \frac{m_q^2}{\bar{x}^2} (1 + \lambda_1 h') \right] \delta_{h',h''} + 2\lambda_1 \bar{\theta} \frac{m_q}{\omega} \delta_{h',-h''} \right\}, \end{aligned} \quad (27)$$

where $\bar{x} = \bar{p}_0/\omega$, and $\omega = \sqrt{s}/2$ is the photon energy in the $\gamma\gamma$ c.m. frame. If we note that the polarization of the incoming quark is

$$\zeta = \frac{\text{Tr}(\boldsymbol{\sigma}\bar{\rho})}{\text{Tr}(\bar{\rho})},$$

then the longitudinal component is given by

$$\zeta_L = \frac{\bar{\rho}^{1,1} - \bar{\rho}^{-1,-1}}{\bar{\rho}^{1,1} + \bar{\rho}^{-1,-1}}. \quad (28)$$

We are now ready to turn to the head-on Compton scattering of the photon $\gamma(\lambda, k_2)$ on the longitudinally polarized quark $q(\zeta_L, k_1 - p)$. In the limit $m_q \rightarrow 0$ it can be shown (see, for example [30])

$$\sum_{\substack{\lambda_g, h \\ \text{colours}}} \left| \overline{M} \left(\gamma(\lambda) q(\zeta_L) \rightarrow q(h) g(\lambda_g) \right) \right|^2 = 2C_F(4\pi)^2 \alpha\alpha_S Q_q^2 \left[\frac{\kappa_2}{\kappa_1} + \frac{\kappa_1}{\kappa_2} + \zeta_L \lambda \left(\frac{\kappa_1}{\kappa_2} - \frac{\kappa_2}{\kappa_1} \right) \right], \quad (29)$$

where $C_F = (N_c^2 - 1)/2N_c = \frac{4}{3}$ and

$$\kappa_1 = k_2 \cdot (k_1 - \bar{p}), \quad \kappa_2 = (k_2 \cdot p). \quad (30)$$

It is easy to show that

$$\frac{\kappa_2}{\kappa_1} \simeq \frac{\omega - p_0}{\bar{p}_0} = \frac{1-x}{\bar{x}} \quad (31)$$

with $x = p_0/\omega$ and

$$1 + \cos\theta = \frac{2(1-x)}{\bar{x}} \frac{(1-\bar{x})}{x} \quad (32)$$

where θ is the polar angle between the momenta \mathbf{k}_1 of the incoming photon and \mathbf{p} of the outgoing quark in the overall cms. Note that Eq. (29) includes the sum over the final and the average over the initial colour states.

Using (23), (26) and (29) we find that the contribution to the cross section from the Compton regime shown in Fig. 2 is

$$\begin{aligned} \frac{d\sigma_{\text{Compton}}}{d\cos\theta} &= \int \frac{d^3\bar{p}}{(2\pi)^2 2\bar{p}_0} \frac{\alpha\alpha_S C_F(1-\bar{x}) Q_q^2}{2\omega^2[2-\bar{x}(1-\cos\theta)]^2} \\ &\left[\text{Tr}(\bar{\rho}) \left(\frac{\kappa_2}{\kappa_1} + \frac{\kappa_1}{\kappa_2} \right) + \lambda \text{Tr}(\sigma_3\bar{\rho}) \left(\frac{\kappa_1}{\kappa_2} - \frac{\kappa_2}{\kappa_1} \right) \right]. \end{aligned} \quad (33)$$

If we perform the integration over $d^3\vec{p}$ with the constraint (22) and assume that $\varepsilon_q \ll 1$, then to logarithmic accuracy

$$\frac{d\sigma_{\text{Compton}}}{d\cos\theta} = \frac{\pi\alpha^2 Q_q^4}{\omega^2} \frac{2}{(1+\cos\theta)} \frac{\alpha_S C_F}{\pi} \varepsilon_q \ln\left(\frac{\varepsilon_q M_H}{m_q}\right). \quad (34)$$

Summing over all analogous Compton contributions, we obtain for the final term in (20) the explicit expression

$$\frac{d\sigma_{\text{Compton}}}{d\cos\theta} = \frac{\pi\alpha^2 Q_q^4}{\omega^2 \sin^2\theta} \frac{8\alpha_S C_F}{\pi} \varepsilon_q \ln\left(\frac{\varepsilon_q M_H}{m_q}\right), \quad (35)$$

where α_S is to be evaluated at the hard scale M_H .

4. Physical origin of DL form factors: one-loop approximation

Recall that the m_q^2 suppressed term in (20) contains, in addition to the standard Sudakov-like form factor, a double logarithmic form factor F_q . To leading logarithmic order F_q has the form shown by the series in (21). The resummation of this DL series looks a very difficult task. In this section we describe the physical origin of the form factor F_q and illustrate the derivation of the coefficient c_1 . Then in section 5 we calculate the (positive) c_2 coefficient of the series.

The double logarithmic asymptotics of high energy processes has been the subject of intense study even before the birth of QCD⁷. The most familiar is the so-called Sudakov form factor [24] which occurs if we insist on the suppression of soft collinear radiation. Less frequently we meet other types of DL effects. For instance, specific DL behaviour appears in high energy $e\mu$ backward scattering [34],

$$e(p_1) + \mu(p_2) \rightarrow e(p_3) + \mu(p_4), \quad (36)$$

as exemplified by one-loop diagram of Fig. 3. The analogous process in QCD is the backward scattering of two quarks of different flavour. Here soft fermion propagators play a crucial role, whereas the Sudakov form factor arises from soft photon (or gluon) effects.

It is evident that soft virtual fermions can cause DL effects only in special circumstances. Recall that the boson propagators $D_\gamma, D_g \sim 1/p^2$ while the fermion propagators $D_\ell, D_q \sim 1/\not{p}$ in the massless limit, where p is the particle four momentum. The special feature of high energy $e\mu$ backward scattering is that the four momentum of the incoming $e(\mu)$ essentially coincides with that of the outgoing $\mu(e)$, $p_1 \approx p_4$ and $p_2 \approx p_3$. Hence the momenta of the virtual fermions are approximately equal, $p \approx p'$, and so their propagators double up. Then a DL contribution emerges, after the integration over the soft fermion momenta, in a similar way to the emergence of the Sudakov form factor from the integration over the soft boson momentum. Some interesting applications of these DL effects were originally discussed in [34] for QED, and subsequently in [35, 36] for QCD.

⁷A detailed presentation of DL results in QED is given, for example, in [31, 32] and a comprehensive QCD review in [33].

Here we study another manifestation of DL non-Sudakov effects, namely the form factor F_q in the first term of (20). Thus we are concerned with helicity amplitudes $M_{\lambda,\lambda}^{h,h}$ which contain an m_q suppression factor. To obtain the DL contribution we therefore keep m_q in one of the fermion propagators which makes the behaviour $m_q/(p^2 - m_q^2)$ similar to that of the boson propagator⁸.

From the physical point of view the appearance of a new type of DL effects in matrix elements with helicity violation is connected with behaviour of the basic QCD (or QED) transition amplitudes. First, helicity-violating $g \rightarrow q\bar{q}$ or $q \rightarrow qg$ amplitudes do not vanish when the momenta of the particles become parallel, unlike the helicity-conserving case, as is clear from angular momentum conservation. Secondly, these helicity-violating amplitudes depend on the energy ε of the softest quark (anti-quark) as $m_q/\sqrt{\varepsilon}$ (supposing, of course, that $\varepsilon \gg m_q$), whereas the vertices with helicity conservation behave as $\sqrt{\varepsilon}$. Therefore, in order to have DL effects due to the soft quark it must propagate between two vertices, one of which is helicity-violating. Of course, we need large invariant masses of any pair of other particles entering the different vertices. Fig. 1 exemplifies such a situation.

In the Feynman gauge the diagram in Fig. 1 also gives a DL contribution from soft gluon exchange. However, soft gluon and soft quark DL effects are very different. To understand this difference it is convenient to use a physical gauge. In this gauge it is clear that to give DL effects the gluon must connect two helicity-conserving vertices (because it is soft) and, moreover, the vertices must occur on the same line (in order to generate an angular logarithm). Thus we have a self-energy diagram. Therefore the soft gluon DL effects are related to the real emission of gluons, and we have the well-known cancellation between virtual and real contributions.

On the other hand, soft quark DL effects in helicity-violating processes are not related to real emission and so we have no cancellation. In summary, soft gluon DL effects have a simple probabilistic interpretation while no such picture exists in the case of soft quark DL effects. Rather the latter are essentially interference effects.

To be specific, in this section we calculate the one-loop DL corrections to the dominant amplitude, $M_{\lambda\lambda}^{hh}$ with $h = \lambda$, and leave the two-loop effects to section 5. Recall that the amplitude with $h = -\lambda$ is suppressed by another factor of m_q/M_H , see (7). In fact from now on we shall only consider the case in which the photon and quark (antiquark) helicities are all equal to λ . We will therefore omit the helicity subscripts and superscripts from the amplitudes on the understanding that they are all to be taken equal to λ . Now the box diagram shown in Fig. 1 gives the $\mathcal{O}(\alpha_S)$ contributions to the DL form factors F_g and F_q , where F_g is related to the soft gluon contribution, while F_q corresponds to the soft virtual quark contributions. In general we can evaluate the DL terms by keeping the dependence on the momentum k of the virtual soft parton only in its propagator and in the denominators of the propagators of the virtual particles joined to the soft parton. In the particular case of the $\mathcal{O}(\alpha_S)$ DL corrections to $M(\gamma\gamma \rightarrow q\bar{q})$ this means that we simply have to evaluate the four non-overlapping kinematic

⁸The DL physics here resembles the known case (see e.g. [1, 37]) of the contribution from the light fermion loops ($m_f \ll M_H$) into the $\gamma\gamma$ or gg partial widths of a Higgs boson.

configurations depicted in Fig. 4. The blobs in these four diagrams denote the hard $2 \rightarrow 2$ subprocess and indicate that inside of a blob we can neglect all virtualities of particles external to the blob. Note that in Fig. 4(a) helicity conservation is violated in the hard blob, while in Figs. 4(b-d) the hard blobs conserve helicity and so we can put $m_b = 0$ when calculating them.

It is convenient to write the Born amplitude M_{Born} for central $q\bar{q}$ production in the ultra-relativistic limit in a form,

$$M_{\text{Born}} = -8e^2 Q_q^2 \frac{m_q}{M_H^2} \frac{\mathbf{e}^\lambda(k_1) \cdot \mathbf{e}^\lambda(k_2)}{\sin^2 \theta} \bar{u}^\lambda(p) v^\lambda(\bar{p}), \quad (37)$$

which is independent of the phases of the particle wave functions.

Note that Eq. (7) corresponds to the choice of the polarization vectors $\mathbf{e}^\lambda(k_1)$ and $\mathbf{e}^\lambda(k_2)$ of the incoming photons in the $\gamma\gamma$ c.m. frame with the z axis directed along \mathbf{k}_1 defined as in [31], i.e. for $\lambda = \lambda_1 = \lambda_2 = \pm 1$

$$\begin{aligned} \mathbf{e}^\lambda(k_1) &= -\frac{i\lambda}{\sqrt{2}} (1, i\lambda, 0), \\ \mathbf{e}^\lambda(k_2) &= \mathbf{e}^{-\lambda}(k_1). \end{aligned} \quad (38)$$

For such a choice one has

$$\left(\mathbf{e}^\lambda(k_i)\right)^* = \mathbf{e}^{-\lambda}(k_i); \quad \not{\epsilon}^\lambda(k_2) \not{\epsilon}^{-\lambda}(k_1) = 0, \quad (39)$$

where $\not{\epsilon} \equiv \boldsymbol{\gamma} \cdot \boldsymbol{\epsilon}$. We define the quark and antiquark wavefunctions as

$$\begin{aligned} u^\lambda(p) &= \sqrt{p_0 + m_q} \begin{pmatrix} \phi_\lambda(\mathbf{p}) \\ \lambda |\mathbf{p}| \phi_\lambda(\mathbf{p}) / (p_0 + m_q) \end{pmatrix}, \\ v^\lambda(\bar{p}) &= \sqrt{\bar{p}_0 + m_q} \begin{pmatrix} -\lambda |\bar{\mathbf{p}}| \phi_\lambda(-\bar{\mathbf{p}}) / (\bar{p}_0 + m_q) \\ \phi_\lambda(-\bar{\mathbf{p}}) \end{pmatrix} \end{aligned} \quad (40)$$

where, as usual, we take λ to be the (double) quark helicity, that is

$$\frac{\boldsymbol{\sigma} \cdot \mathbf{p}}{|\mathbf{p}|} \phi_\lambda(\mathbf{p}) = \lambda \phi_\lambda(\mathbf{p}). \quad (41)$$

For virtual gluons we use the Feynman gauge.

The amplitudes corresponding to each of the four diagrams ($i = a, b, c, d$) in Fig. 4 can be written in the factorized form

$$M_i = \mathcal{F}_i M_{\text{Born}}, \quad (42)$$

where \mathcal{F}_i is the form factor from diagram i . We elucidate this result below, taking the diagrams in turn. We stress that each amplitude M_i (apart from M_a) describes the sum of the corresponding diagram in Fig. 4 and the crossed diagram with the photon momenta interchanged, $k_1 \leftrightarrow k_2$.

4.1 The form factor with the $\gamma\gamma \rightarrow q\bar{q}$ hard subprocess

The Sudakov DL effects which arise from the virtual soft gluon are shown in Fig. 4(a). Here, for M_a , the factorized form (42) is immediately evident. In this case

$$\mathcal{F}_a = 4\pi\alpha_S C_F \int \frac{d^4k}{i(2\pi)^4} \frac{-4(p\cdot\bar{p})}{[k^2 - m_g^2 + i\varepsilon][(p+k)^2 - m_q^2 + i\varepsilon][(\bar{p}-k)^2 - m_q^2 + i\varepsilon]}, \quad (43)$$

where $C_F = \frac{4}{3}$ and where a gluon mass m_g is introduced to regularize the infrared singularity. Then, on carrying out the integration in the standard way, we obtain the well known DL result

$$\mathcal{F}_a = -\frac{\alpha_S}{\pi} C_F \left(L_m^2 + L_m \ln \frac{m_q^2}{m_g^2} \right) \quad (44)$$

where we recall that $L_m \equiv \ln(M_H/m_q)$. As usual the infrared divergence $\ln m_g^2$, and also the $\ln^2 m_q^2$ term, cancels after adding the soft real gluon emission contribution. We return to discuss this cancellation at the end of this section.

At first sight the factorized form (42) is not so obvious for diagrams 4(b,c,d) and so we derive it below. Recall that the overall m_q suppression of these amplitudes comes from the fact that only the mass term in the numerator of the propagator $D_q(k) \simeq (\not{k} + m_q)/(k^2 - m_q^2)$ of the soft quark can contribute and we need retain k only in the denominators of the propagators of the virtual particles joined to the soft quark.

4.2 The form factor with the $q\bar{q} \rightarrow q\bar{q}$ hard subprocess

First we study the amplitude corresponding to Fig. 4(b). We may neglect the mass in the numerators of propagators $D_q(k_i)$ of the quarks joined to the soft quark with $i = 1, 2$ and write them as

$$\not{k}_i = \sum_{\lambda} u^{\lambda}(k_i) \bar{u}^{\lambda}(k_i) = \sum_{\lambda} v^{\lambda}(k_i) \bar{v}^{\lambda}(k_i), \quad (45)$$

and use the relations

$$\not{\epsilon}^{\lambda}(k_i) v^{-\lambda}(k_i) = \not{\epsilon}^{\lambda}(k_i) u^{\lambda}(k_i) = \bar{v}^{\lambda}(k_i) \not{\epsilon}^{\lambda}(k_i) = \bar{u}^{-\lambda}(k_i) \not{\epsilon}^{\lambda}(k_i) = 0 \quad (46)$$

in the massless limit. Then it can be easily seen that the amplitude for diagram 4b contains the $q\bar{q} \rightarrow q\bar{q}$ amplitude as a factor. To be precise we have

$$\begin{aligned} M_b &\simeq \left(\frac{\alpha}{\alpha_S} \right) Q_q^2 \mathcal{F}_b M \left(q(k_1, \lambda) + \bar{q}(k_2, \lambda) \rightarrow q(p, \lambda) + \bar{q}(\bar{p}, \lambda) \right) \\ &\times \frac{\bar{u}^{\lambda}(k_1) \not{\epsilon}^{\lambda}(k_1) m_q \not{\epsilon}^{\lambda}(k_2) v^{\lambda}(k_2)}{4C_F(k_1, k_2)} + \left\{ k_1 \leftrightarrow k_2 \right\}. \end{aligned} \quad (47)$$

The summation over the colours of the intermediate $q(k_1, \lambda)$ and $\bar{q}(k_2, \lambda)$ states is implied here. The effect is to cancel the factor C_F in the denominator. This enables us to have the same normalisation of the form factors \mathcal{F}_i of diagrams 4(a,b,c). Due to the conservation of colour

only the scattering diagram (and not the annihilation diagram) contributes to $M(q\bar{q} \rightarrow q\bar{q})$ in (47). Note that the annihilation channel is also suppressed due to helicity conservation.

The DL factor in (47) is given by

$$\begin{aligned} \mathcal{F}_b &= 4\pi\alpha_S(M_H)C_F \int \frac{d^4k}{i(2\pi)^4} \frac{-4(k_1.k_2)}{[k^2 - m_q^2 + i\varepsilon][(k_1+k)^2 - m_q^2 + i\varepsilon][(k_2-k)^2 - m_q^2 + i\varepsilon]} \\ &= -\frac{\alpha_S(M_H)}{\pi} C_F L_m^2 \equiv \mathcal{F}. \end{aligned} \quad (48)$$

To reduce (47) to the factorized form given in (42) we rewrite the $M(q\bar{q} \rightarrow q\bar{q})$ scattering amplitude using the Fierz transformation (which is especially simple when the particles have the same helicities)

$$(\bar{u}_1^\lambda \gamma^\mu u_2^\lambda)(\bar{v}_3^\lambda \gamma_\mu v_4^\lambda) = 2(\bar{u}_1^\lambda v_4^\lambda)(\bar{v}_3^\lambda u_2^\lambda). \quad (49)$$

Then the numerator in (47) can be rearranged to contain the factor

$$\text{Tr}\left(\not{k}_1 \not{\epsilon}^\lambda(k_1) \not{\epsilon}^\lambda(k_2) \not{k}_2(1 + \lambda\gamma_5)\right) \bar{u}^\lambda(p) v^\lambda(\bar{p}) = -8(k_1.k_2) \left(e^\lambda(k_1) \cdot e^\lambda(k_2)\right) \bar{u}^\lambda(p) v^\lambda(\bar{p}). \quad (50)$$

If we use this result, together with (37), we find (47) has the factorized form given in (42) for $i = b$.

4.3 The form factors for the Compton scattering hard subprocesses

We now turn to the final two diagrams of Fig. 4. Noting the conservation of quark helicity in the hard process, we obtain

$$\begin{aligned} M_c &= \sqrt{\frac{\alpha}{\alpha_S}} Q_q \mathcal{F}_c M^\mu \left(\gamma(k_1, \lambda) + q(k_2, \lambda) \rightarrow q(p, \lambda) + g(\bar{p}, \mu) \right) \\ &\times \frac{\bar{u}^\lambda(k_2) \not{\epsilon}^\lambda(k_2) m_q \gamma_\mu v^\lambda(\bar{p})}{4C_F(\bar{p}.k_2)} + \left\{ k_1 \leftrightarrow k_2 \right\}. \end{aligned} \quad (51)$$

where M^μ is the Compton ($\gamma q \rightarrow qg$) amplitude for a gluon with polarization index μ . Once again a summation of the colours of the intermediate particles (the quark and the gluon) is implied. Again it leads to a cancellation of the colour factor C_F shown in (51). The form factor \mathcal{F}_c is given by

$$\mathcal{F}_c = 4\pi\alpha_S C_F \int \frac{d^4k}{i(2\pi)^4} \frac{4(k_2.\bar{p})}{[k^2 - m_q^2 + i\varepsilon][(k_2+k)^2 - m_q^2 + i\varepsilon][(\bar{p}+k)^2 + i\varepsilon]}. \quad (52)$$

It is useful to note that in the one-loop approximation only the s -channel diagram contributes to the amplitude for the Compton scattering. The u -channel contribution vanishes in this approximation due to relation

$$2\gamma^\mu u^\lambda(k_2) \bar{u}^\lambda(k_2) \not{\epsilon}^\lambda(k_2) \gamma_\mu = \gamma^\mu \not{k}_2(1 - \lambda\gamma_5) \not{\epsilon}^\lambda(k_2) \gamma_\mu = 4(1 - \lambda\gamma_5)(k_2.e^\lambda(k_2)) = 0. \quad (53)$$

However, in higher order one has to take into account both the s and u channel contributions.

It is easy to see that both diagram 4c and the crossed ($k_1 \leftrightarrow k_2$) diagram contain DL factors which, to DL accuracy, are equal to each other. Moreover the integrands in (48) and (52) are related by the interchange

$$k_1 \leftrightarrow -\bar{p}, \quad k \rightarrow -k. \quad (54)$$

To the accuracy to which we are working, the absence of m_q^2 in the third factor of the denominator in (52) is not important. Thus we have

$$\mathcal{F}_c = -\frac{\alpha_S}{\pi} C_F L_m^2 = \mathcal{F}. \quad (55)$$

Note that for \mathcal{F}_c (and also $\mathcal{F}_{a,d}$) we have no reason to evaluate α_S at the hard scale M_H , although in the following we shall not take into account possible differences in the scale of α_S for the different \mathcal{F}_i . If we manipulate the spinor structure in (51), just as we did for the previous case of amplitude M_b , then we obtain the factorized form (42) for M_c also. By repeating the same procedure, it is straightforward to show that the factorized form (42) follows for the amplitude M_d as well and that

$$\mathcal{F}_d = \mathcal{F}_c = \mathcal{F}. \quad (56)$$

It is worth drawing attention to one subtlety. We had noted that the amplitude M_b contained as one of the factors the physical $q\bar{q} \rightarrow q\bar{q}$ amplitude with the same helicities for the incoming and outgoing quarks, see (47). The same is not true for M_c . In (51) we sum over all the gluon polarization states, including the non-physical ones. However, it is possible to restore the symmetry of the helicity structure of M_c to that of M_b if we exploit the fact that both $M^\mu(\gamma q \rightarrow qg)$ and its spinor multiplier in (51) vanish if multiplied by \bar{p}_μ . The former follows from gauge invariance, $\bar{p}_\mu M^\mu = 0$ and the latter is a consequence of the Dirac equation for $v^\lambda(\bar{p})$. Thus we need only sum over the physical gluon polarization states $e_\mu^\lambda(\bar{p})$, which satisfy

$$\not{\epsilon}^{-\lambda}(\bar{p}) v^\lambda(\bar{p}) = 0. \quad (57)$$

This condition is gauge invariant and it can be derived in the same way as (46). Using these results we can rearrange (51) into the form

$$\begin{aligned} M_c &= -\sqrt{\frac{\alpha}{\alpha_S}} Q_q \mathcal{F}_c M\left(\gamma(k_1, \lambda) + q(k_2, \lambda) \rightarrow q(p, \lambda) + g(\bar{p}, \lambda)\right) \\ &\times \frac{\bar{u}^\lambda(k_2) \not{\epsilon}^\lambda(k_2) m_q \not{\epsilon}^\lambda(\bar{p}) v^\lambda(\bar{p})}{4C_F(\bar{p}, k_2)} + \left\{ k_1 \leftrightarrow k_2 \right\} \end{aligned} \quad (58)$$

in which we keep only the contribution corresponding to a gluon of helicity λ .

Before proceeding to the study of higher loop contributions in section 5, note that although the derivation of the factorized form (42) for the amplitudes $M_{b,c,d}$ was given in a way that allowed a clear physical interpretation, it is probable that there is a more general reason for

this result. It could well be that factorized relations of the type shown in (47) and (58) are the result of (super)symmetry relations between amplitudes with the same values of the helicities (and doubled helicities) of the bosons (and fermions) participating in the hard scattering.

4.4 Expressions for the form factors F_g and F_q

We return to the calculation of the one-loop correction to the cross section. On account of the factorized form (42), the one-loop virtual corrections give a factor $(1 + \delta_V)$ in the formula for the cross section, where

$$\delta_V = 2 \sum_{i=a,b,c,d} \mathcal{F}_i. \quad (59)$$

We must combine this correction with the contribution from soft real gluon emission. Now the amplitude $M^{(1)}$ describing the emission of *one* soft gluon of momentum k_g is

$$M^{(1)} = M_{\text{Born}} g_S \langle t^a \rangle e_\mu(k_g) J^\mu(k_g) \quad (60)$$

with

$$J^\mu(k) = \frac{p^\mu}{p \cdot k} - \frac{\bar{p}^\mu}{\bar{p} \cdot k}, \quad (61)$$

where e_μ is the polarisation vector of the emitted gluon; and p, \bar{p} are the momenta of outgoing quark and antiquark. The gluon has colour index a , and $\langle t^a \rangle$ denotes the generator of the fundamental representation of the colour group evaluated between the q and \bar{q} states. Therefore the correction to the cross section due to real emission is

$$\begin{aligned} \delta_R &= g_S^2 C_F \int_{\Omega_R} \frac{d^3 k}{(2\pi)^3 2\omega} (-J_\mu(k) J^\mu(k)) \\ &= \frac{\alpha_S C_F}{4\pi^2} \int_{\Omega_R} \frac{d^3 k}{\omega} \frac{2(p \cdot \bar{p})}{(k \cdot p)(k \cdot \bar{p})}, \end{aligned} \quad (62)$$

with $\omega = (\mathbf{k}^2 + m_g^2)^{\frac{1}{2}}$, and where Ω_R denotes the region of phase space of gluon radiation allowed by the cut-off prescription.

The infrared divergence in δ_R cancels that of the virtual contribution $2\mathcal{F}_a$ in (59). Indeed the sum $\delta_R + 2\mathcal{F}_a$ represents the first term of the expansion of the Sudakov form factor F_g which occurs in (17) and (20). Hence we have

$$F_g = \exp(\delta_R + 2\mathcal{F}_a). \quad (63)$$

For the non-Sudakov form factor F_q we have, in the one-loop approximation,

$$F_q = 1 + 2 \sum_{i=b,c,d} \mathcal{F}_i = 1 + 6\mathcal{F} = 1 - \frac{8\alpha_S}{\pi} L_m^2. \quad (64)$$

where we have used (48), (55) and (56). That is we have reproduced the result that was first derived in Ref. [21].

Let us now give the explicit expressions for the Sudakov form factor F_g for the different cut-off prescriptions. When we impose the ε_g restriction (12) on the gluon transverse energy we obtain

$$\delta_R(\varepsilon_g) = -2\mathcal{F}_a - 2 \frac{\alpha_S C_F}{\pi} L_g^2 \quad (65)$$

for $|k_{g\perp}| = \Delta E_g \gtrsim m_q$, where logarithmic factor L_g is defined in (18). Thus on combining δ_R with δ_V of (59) we see that (63) becomes

$$F_g(\varepsilon_g) = \exp\left(-\frac{2\alpha_S}{\pi} C_F L_g^2\right). \quad (66)$$

On the other hand if we restrict the gluon momentum by $k_g \leq k_0$, then

$$\delta_R(k_0) = -2\mathcal{F}_a - 4 \frac{\alpha_S C_F}{\pi} L_m L_0, \quad (67)$$

where now the logarithmic factors are defined in (19). In this case we see that (63) is of the form

$$F_g(k_0) = \exp\left(-\frac{4\alpha_S}{\pi} C_F L_m L_0\right). \quad (68)$$

Finally, let us present the expression for the Sudakov form factor in terms of the standard jet-finding parameter y_{cut} used in Refs. [18] - [23]. By imposing the constraint

$$(p(\bar{p}) + k_g)^2 < y_{\text{cut}} s \quad (69)$$

on the process $\gamma\gamma \rightarrow q\bar{q}g$ at the partonic level we can write down the one-loop real correction δ_R as

$$\delta_R(y_{\text{cut}}) = -2\mathcal{F}_a - \frac{\alpha_S C_F}{\pi} \ln^2 \frac{1}{y_{\text{cut}}}. \quad (70)$$

Then (63) becomes

$$F_g(y_{\text{cut}}) = \exp\left(-\frac{\alpha_S}{\pi} C_F \ln^2 \frac{1}{y_{\text{cut}}}\right). \quad (71)$$

where we have assumed that $y_{\text{cut}} \gg m_q^2/s$. Recall that in the case of form factor F_g there is no reason to evaluate α_S at the hard scale M_H .

5. The two-loop approximation for $\gamma\gamma \rightarrow q\bar{q}$

In this section we study the two-loop approximation to the cross section for the central production of a $q\bar{q}$ pair in the collision of photons with equal helicities. Of course, $q\bar{q}$ production can be accompanied by other final state particles, depending on the experimental conditions. Here we adopt restrictive experimental criteria so as to provide conditions that are most favourable for the detection of the Higgs boson. This means that, besides the $q\bar{q}$ pair, the final state contains only soft gluons. Therefore the two-loop contribution to the $J_z = 0$ cross section that we are interested in may be written in the form

$$d\sigma_{2\text{-loop}} = d\sigma_{\text{Born}}(\gamma\gamma \rightarrow q\bar{q}gg) + d\sigma_{1\text{-loop}}(\gamma\gamma \rightarrow q\bar{q}g) + d\sigma_{2\text{-loop}}(\gamma\gamma \rightarrow q\bar{q}), \quad (72)$$

where the emitted gluons are soft. We evaluate the three components in turn.

5.1 The contribution from $\gamma\gamma \rightarrow q\bar{q}gg$

There are two types of DL contribution to the two-gluon emission component of the cross section of (72) in the double logarithm approximation. The first part, part A, comes when the emitted gluons are strongly ordered in angle. It is similar to the QED case and has amplitude

$$M_A^{(2)} = M_{\text{Born}} g_S^2 e_\mu(k_{1g}) J^\mu(k_{1g}) e_\mu(k_{2g}) J^\mu(k_{2g}) C(a_1, a_2), \quad (73)$$

where the superscript (2) denotes the emission of *two* soft gluons and where J^μ is defined in (61). The colour factor

$$C(a_1, a_2) = \begin{cases} \langle t^{a_1} t^{a_2} \rangle & \text{if } \theta_1 \ll \theta_2 \\ \langle t^{a_2} t^{a_1} \rangle & \text{if } \theta_2 \ll \theta_1, \end{cases} \quad (74)$$

where a_i are the colour labels of the emitted gluons and θ_i is the angle of the i -th gluon with respect to the quark momentum \mathbf{p} . In both cases when $|C|^2$ is summed over the colours of the emitted gluons we obtain C_F^2 . Thus part A of the cross section is

$$d\sigma_{\text{Born}}^A(\gamma\gamma \rightarrow q\bar{q}gg) = d\sigma_{\text{Born}}(J_z = 0) \frac{\delta_R^2}{2}, \quad (75)$$

where δ_R is given by (62).

However, unlike QED, there is another region which leads to a double logarithmic contribution to the cross section. Namely the region in which the emission of the two gluons is strongly correlated so that the angle between their momenta is much less than the angles of their emission with respect to the quark or antiquark. The amplitude in this case (part B) is

$$M_B^{(2)} = M_{\text{Born}} g_S^2 \frac{e_\mu(k_{1g}) J^\mu(k_{1g}) e_\mu(k_{2g}) k_{1g}^\mu}{(k_{1g} \cdot k_{2g})} i f_{a_1 a_2 a} \langle t^a \rangle, \quad (76)$$

where f_{abc} is the usual QCD structure constant, and where we have assumed that the gluon energies satisfy $\omega_{1g} \gg \omega_{2g}$. Note that physical polarisation vectors have been used for the second gluon in (76) which satisfy $e(k_{2g}) \cdot k_{2g} = 0$. The contribution to the cross section from this region, region B, with two soft gluons emitted is

$$\begin{aligned} d\sigma_{\text{Born}}^B(\gamma\gamma \rightarrow q\bar{q}gg) &= d\sigma_{\text{Born}}(J_z = 0) \frac{\alpha_S C_F}{4\pi^2} \\ &\times \int_{\Omega_R} \frac{d^3k}{\omega} \frac{2(p \cdot \bar{p})}{(k \cdot p)(k \cdot \bar{p})} \frac{\alpha_S C_A}{4\pi} \ln^2 \left(\frac{(k \cdot p)(k \cdot \bar{p})}{m_g^2(p \cdot \bar{p})} \right), \end{aligned} \quad (77)$$

where $C_A = N_c = 3$. The total $\gamma\gamma \rightarrow q\bar{q}gg$ cross section is the sum of (75) and (77),

$$d\sigma_{\text{Born}}(\gamma\gamma \rightarrow q\bar{q}gg) = d\sigma_{\text{Born}}^A + d\sigma_{\text{Born}}^B. \quad (78)$$

5.2 The two-loop contribution from $\gamma\gamma \rightarrow q\bar{q}g$

The component of the two-loop cross section (72) which arises from the emission of a single soft gluon comes from the interference of $M_{1\text{-loop}}^{(1)}$ with its Born value $M^{(1)}$ given in (60). Recall that the superscript (1) denotes the emission of a *single* soft gluon. Thus we have to calculate the one-loop correction of the Born amplitude $M^{(1)}$ for the process $\gamma\gamma \rightarrow q\bar{q}g$. In the Born approximation the double logarithmic contribution to the cross section comes from regions where the soft gluon is emitted quasi-collinearly with either the outgoing quark or antiquark. Because the contributions for emission along the quark or antiquark direction are equal, we could restrict ourselves to considering the region of quasi-collinearity with the quark. However, we shall not do this in order to obtain a general picture and to maintain gauge invariance.

Just as we did in the calculation of the one-loop correction to the matrix element of the basic $\gamma\gamma \rightarrow q\bar{q}$ process, we separate the ‘‘hard’’ stage of the process from the ‘‘soft’’ stage. The later stage leads to double logarithmic corrections. The gluon is emitted in the soft stage. In the cases when the ‘‘hard’’ subprocesses do not coincide with the basic process (namely for Figs. 4(b-d)) the appropriate diagrams are obtained by the addition of a gluon line to all the diagrams of Figs. 4(b-d), noting that it cannot be emitted from the ‘‘hard blob’’. But such a statement is not correct for the case of the ‘‘hard’’ $\gamma\gamma \rightarrow q\bar{q}$ process of Fig. 4(a). The reason for this difference is evident. In the latter case, contrary to the former ones, there are other one-loop diagrams besides those shown in Fig. 4 (for example, diagrams with self-energy insertions). We did not consider them because they do not give DL contributions (in the Feynman gauge which we use here). But after the addition of the real soft gluon line they can give such a contribution.

In fact, the case of the ‘‘hard’’ $\gamma\gamma \rightarrow q\bar{q}$ process of Fig. 4(a) is analogous to the decay of a ‘‘heavy’’ photon into a $q\bar{q}$ pair [38]. The contributing diagrams are shown in Fig. 5. We also have diagrams 5(\bar{a} , \bar{b} , \bar{d}) in which the soft gluon is emitted from the \bar{q} rather than the q . The evaluation of these seven diagrams is similar to that performed in [38]. The result is

$$M_{1\text{-loop}}^{(1)\text{ Fig.5}} = M_{\text{Born}} g_S \langle t^a \rangle e_\mu(k_g) J^\mu(k_g) \left[\mathcal{F}_a - \frac{\alpha_S}{2\pi} \frac{C_A}{4} \ln^2 \left(\frac{(k_g \cdot p)(k_g \cdot \bar{p})}{m_g^2(p \cdot \bar{p})} \right) \right], \quad (79)$$

where \mathcal{F}_a is given by (44), J^μ by (61) and m_g is the ‘mass’ of the gluon. Note that the second term in the square brackets violates the soft emission factorization and Poisson distribution theorems that hold for QED [38].

Next we consider the gluon emission in the case of the ‘‘hard’’ $q\bar{q} \rightarrow q\bar{q}$ process of Fig. 4(b). The diagrams are displayed in Fig. 6. Again we must also include the contribution of diagram 6(\bar{a}) in which the gluon is emitted from the \bar{q} . The evaluation of the diagrams, together with the crossed diagrams with $k_1 \leftrightarrow k_2$, is non-trivial and introduces novel features. The derivation is described in Appendix A. The final result can be presented in the form of Eq. (47) with the replacements

$$M_b \rightarrow M_{1\text{-loop}}^{(1)\text{ Fig.6}},$$

$$\mathcal{F}_b \rightarrow g_S \langle t^a \rangle \left[e_\mu(k_g) J^\mu(k_g) \mathcal{F}_b + i\lambda \frac{\varepsilon_{\mu\nu\rho\sigma} k_2^\mu k_1^\nu e^\rho(k_g) k_g^\sigma}{(k_g \cdot k_1)(k_g \cdot k_2)} \left(\frac{-\alpha_S}{4\pi} \right) \left(C_F - \frac{C_A}{2} \right) \ln^2 \left(\frac{(k_g \cdot k_1)(k_g \cdot k_2)}{m_q^2 (k_1 \cdot k_2)} \right) \right], \quad (80)$$

where \mathcal{F}_b on the right hand side is given by (48), $\varepsilon_{\mu\nu\rho\sigma}$ is the totally antisymmetric tensor, $\varepsilon_{0123} = 1$, and λ specifies the helicity of all the $\gamma\gamma \rightarrow q\bar{q}$ particles. The first term in the square brackets is standard. It arises from diagrams 6(a, \bar{a}). It is worth noting that the $\varepsilon_{\mu\nu\rho\sigma}$ term, which contains correlations involving the photon helicities, are coloured suppressed by $\mathcal{O}(1/N_c^2)$ compared to the standard QED-like terms. Let us emphasise that this term should be retained only when $(k_g \cdot k_1)(k_g \cdot k_2) \gg m_q^2(k_1 \cdot k_2)$. It is also assumed here and in what follows that each term containing a logarithmic factor should be retained only when the argument of this logarithm is large.

Figs. 6(b,c,d), and their $k_1 \leftrightarrow k_2$ counterparts, have contributions proportional to

$$e(k_g) \cdot k_i / (k_g \cdot k_i) \quad (81)$$

with $i = 1, 2$, which cancel when we take the sum. The cancellation could be naively expected since collinear photon-gluon singularities are clearly unphysical. However, diagram 6(d) also gives rise to the final term in (80). This is a novel contribution. Evidently its appearance is connected with the peculiarity of processes with helicity violation. Due to the presence of $\varepsilon_{\mu\nu\rho\sigma}$ this contribution is antisymmetric with respect to the interchange $k_1 \leftrightarrow k_2$. However, symmetry of \mathcal{F}_b was necessary to obtain the factorized form (42) from (47). As a consequence diagrams 6(b,c,d) considered together with the crossed diagrams ($k_1 \leftrightarrow k_2$) do not have the factorized form shown in (42).

We now turn to the corrections to diagram 4(c) with the ‘‘hard’’ Compton subprocess $\gamma q \rightarrow qg$. In this case the resulting diagrams for the gluon emission are shown in Fig. 7. The structure of the final result from the sum of these diagrams is similar to that obtained from the diagrams of Fig. 6. It is derived in Appendix A and corresponds to making the replacements

$$M_c \rightarrow M_{1\text{-loop}}^{(1)\text{Fig.7}},$$

$$\mathcal{F}_c \rightarrow g_S \langle t^a \rangle \left[e_\mu(k_g) J^\mu(k_g) \mathcal{F}_c + i\lambda \frac{\varepsilon_{\mu\nu\rho\sigma} \bar{p}^\mu k_2^\nu e^\rho(k_g) k_g^\sigma}{(k_g \cdot k_2)(k_g \cdot \bar{p})} \left(\frac{-\alpha_S}{4\pi} \right) \left(C_F - \frac{C_A}{2} \right) \ln^2 \left(\frac{(k_g \cdot \bar{p})(k_g \cdot k_2)}{m_q^2 (k_2 \cdot \bar{p})} \right) \right] \quad (82)$$

in (51). Here λ is the helicity, J^μ is defined by (61) and \mathcal{F}_c on the right hand side is given by (55). Now the first term comes not only from the diagrams shown in Figs. 7(a,b), but includes contributions proportional to $(e_\mu(k_g) \cdot \bar{p}) / (k_g \cdot \bar{p})$ coming from the diagrams of Figs. 7(d,e) as

well. The contributions of the type (81) from the diagrams of Figs. 7(c,e) and their $k_1 \leftrightarrow k_2$ counterparts cancel just as in the previous case. The final term comes from the diagram of Fig. 7(e).

Finally we consider the soft gluon emission in the “hard” Compton subprocess $\gamma\bar{q} \rightarrow \bar{q}g$ of Fig. 4(d). This contribution is exactly analogous to the previous one and can be obtained by making in (82) the replacements

$$\mathcal{F}_c \rightarrow \mathcal{F}_d, \quad \bar{p} \leftrightarrow -p, \quad k_2 \rightarrow k_1 \quad (83)$$

and changing the overall sign. Note, however, that $\mathcal{F}_d = \mathcal{F}_c = \mathcal{F}$, see (56), and that $J^\mu(k_g)$ (61) remains unchanged after these operations.

So, if we were to omit the $\varepsilon_{\mu\nu\rho\sigma}$ terms, we see that the total contribution of the “hard” quark-quark and Compton subprocesses would have a simple factorized form given by the product of three factors: the Born matrix element of the basic process $\gamma\gamma \rightarrow q\bar{q}$, the one-loop correction \mathcal{F}_i coming from the diagrams 4(b-d), and the factor $g_S \langle t^a \rangle e_\mu(k_g) J^\mu$ for the accompanying gluon bremsstrahlung. But it now seems at first sight that the presence of the $\varepsilon_{\mu\nu\rho\sigma}$ terms will destroy even the factorization of the Born amplitude of the basic process. However, we will find that this is not the case.

A second apparent problem is that the regions of quasi-collinearity of the emitted gluon with the momenta of the initial photons give singularities in the separate contributions (80), (82) and (83). However, these singularities cancel when we take the sum of the contributions, as one can naively expect from the physical point of view. The cancellation can be demonstrated by using the general generic expression

$$f(p_1, p_2, e, k_g) = \frac{\varepsilon_{\mu\nu\rho\sigma} p_1^\mu p_2^\nu e^\rho k_g^\sigma}{(k_g \cdot p_1)(k_g \cdot p_2)} \ln^2 \left(\frac{(k_g \cdot p_1)(k_g \cdot p_2)}{m_q^2(p_1 \cdot p_2)} \right), \quad (84)$$

where the momenta p_1, p_2 are k_2, k_1 in (80), \bar{p}, k_2 in (82) and k_1, p in (83). Now in the region where the gluon emission is quasi-collinear with p_1 , say, that is where angle $(\mathbf{k}_g, \mathbf{p}_1) \ll$ angle $(\mathbf{p}_2, \mathbf{p}_1)$ it is easy to show that

$$f(p_1, p_2, e, k_g) \simeq - \frac{(\mathbf{e} \times \hat{\mathbf{k}}_g) \cdot \mathbf{p}_1}{(k_g \cdot p_1)} \ln^2 \left(\frac{(k_g \cdot p_1)\omega_g}{m_q^2 E_1} \right), \quad (85)$$

where $\hat{\mathbf{k}}_g \equiv \mathbf{k}_g/\omega_g$. Note that f in (85) is independent of p_2 . Moreover note the equality of the coefficient functions of \mathcal{F}_i in the uncrossed terms in (47) for M_b , in (58) for M_c and the analogous equation for M_d . The proof follows as a by-product of the demonstration of the equality of the sum of the crossed and uncrossed terms used in derivation of factorization formula (42). Using the above properties we can combine together the corrections (79), (80), (82) and (83) to obtain

$$\begin{aligned} M_{1\text{-loop}}^{(1)} &= M_{\text{Born}} g_S \langle t^a \rangle \left[e_\mu(k_g) J^\mu \left\{ \mathcal{F}_a + 3\mathcal{F} - \frac{\alpha_S}{8\pi} C_A \ln^2 \left(\frac{(k_g \cdot p)(k_g \cdot \bar{p})}{m_q^2(p \cdot \bar{p})} \right) \right\} \right. \\ &+ \left. i\lambda \frac{\varepsilon_{\mu\nu\rho\sigma} \bar{p}^\mu p^\nu e^\rho(k_g) k_g^\sigma}{(k_g \cdot \bar{p})(k_g \cdot p)} \left(\frac{-\alpha_S}{4\pi} \right) \left(C_F - \frac{C_A}{2} \right) \ln^2 \left(\frac{(k_g \cdot p)(k_g \cdot \bar{p})}{m_q^2(p \cdot \bar{p})} \right) \right], \quad (86) \end{aligned}$$

where m_g and λ denote respectively the gluon mass and $\gamma\gamma \rightarrow q\bar{q}$ particle helicities. The absence of the singularities when the gluon becomes collinear with either of the initial photons is now clearly manifest.

The presence of the $\varepsilon_{\mu\nu\rho\sigma}$ term in the one-loop correction to the gluon emission amplitude (86) demonstrates the non-triviality of physical phenomena of helicity-violating processes. Fortunately this term does not contribute in the approximation (72) that we are studying. It is pure imaginary with respect to the Born amplitude (60) for $\gamma\gamma \rightarrow q\bar{q}g$ and so it makes no contribution to $d\sigma_{1\text{-loop}}(\gamma\gamma \rightarrow q\bar{q}g)$ of (72). This component of the cross section is therefore given by

$$d\sigma_{1\text{-loop}}(\gamma\gamma \rightarrow q\bar{q}g) = d\sigma_{\text{Born}}(J_z = 0) \frac{\alpha_S C_F}{4\pi^2} \times \int_{\Omega_R} \frac{d^3k}{\omega} \frac{2(p\cdot\bar{p})}{(k\cdot p)(k\cdot\bar{p})} \left[2(\mathcal{F}_a + 3\mathcal{F}) - \frac{\alpha_S}{4\pi} C_A \ln^2 \left(\frac{(k\cdot p)(k\cdot\bar{p})}{m_g^2(p\cdot\bar{p})} \right) \right]. \quad (87)$$

Note that the last term of (87) precisely cancels the contribution (77) from the emission of two gluons with strongly correlated momenta that we discussed in section 5.1. Therefore summing up the contributions (75), (77) and (87) of the inelastic processes to the cross section (72) we obtain the following remarkably simple result

$$d\sigma_{\text{Born}}(\gamma\gamma \rightarrow q\bar{q}gg) + d\sigma_{1\text{-loop}}(\gamma\gamma \rightarrow q\bar{q}g) = d\sigma_{\text{Born}}(J_z = 0) \left[\frac{1}{2} \delta_R^2 + 2\delta_R (\mathcal{F}_a + 3\mathcal{F}) \right], \quad (88)$$

where δ_R is given by (62) (or, more precisely, (65), (67) or (70)), \mathcal{F}_a by (44) and $\mathcal{F} = \mathcal{F}_b = \mathcal{F}_c = \mathcal{F}_d$ by (48).

5.3 The non-radiative two-loop contribution

We now come to the last term in (72), namely the two-loop contribution, $d\sigma_{2\text{-loop}}(\gamma\gamma \rightarrow q\bar{q})$, to the cross section of the basic process. It consists of two pieces. The first is the square of the one-loop corrections, $(M_a + M_b + M_c + M_d)$, to the basic matrix element

$$d\sigma_{2\text{-loop}}^{(1)}(\gamma\gamma \rightarrow q\bar{q}) = d\sigma_{\text{Born}}(J_z = 0) \left(\sum_i \mathcal{F}_i \right)^2, \quad (89)$$

see (42). The \mathcal{F}_i are given by (44), (48), (55) and (56).

The second piece comes from the interference of the two-loop correction to the matrix element with its Born value (37). The calculation can be performed in a similar way to that used in the previous section. Again we separate the ‘‘hard’’ and ‘‘soft’’ stages of the process. The soft stage is the source of the DL contributions whereas, by dimensional arguments, we find that the hard stage is a two-to-two process. Therefore we have the same possibilities as for the one-loop correction (see Fig. 4). The DL contributions can come from either a soft gluon or a soft quark, but the quark can only occur once since it leads to a m_q/M_H suppression of

the amplitude (which is the usual suppression of the helicity violating amplitudes). Therefore, two-loop DL corrections can be obtained from the diagrams of Fig. 4 by the insertion of a soft gluon line. We call these soft insertions. Of course we do not have to consider a soft gluon emitted from the “hard blob”.

If the hard process is $\gamma\gamma \rightarrow q\bar{q}$ then its dominant amplitude $M_{\lambda,\lambda}^{\lambda,\lambda}$ is already suppressed by m_q/M_H (see (7)), and so the DL contributions come only from soft gluons. Due to the factorization of the hard part of the matrix element this case is exactly analogous to the quark form factor. The diagrams are obtained by soft insertions in Fig. 4(a). In the Feynman gauge (which is used for virtual gluons) the DL contributions only occur when the soft gluon connects lines with strongly different momenta, that is momenta p_i and p_j which satisfy

$$|p_i \cdot p_j| \gg |p_i^2|, |p_j^2|. \quad (90)$$

The contributing diagrams, shown in Fig.8, give in total

$$M_{2\text{-loop}}^{\text{Fig.8}} = M_{\text{Born}} \frac{\mathcal{F}_a^2}{2}. \quad (91)$$

If the hard process is $q\bar{q} \rightarrow q\bar{q}$ then we must make soft insertions in Fig. 4(b). Since the DL contributions only occur when the soft gluon connects line with strongly different momenta we need only consider the diagrams shown in Fig. 9. We discuss the details in Appendix B. The final result is that diagrams 9(g) and 9(h) do not contribute, while 9(c) - 9(f) cancel each other. Therefore the net contribution comes only from diagrams 9(a,b) and is equal to

$$M_{2\text{-loop}}^{\text{Fig.9}} = M_{\text{Born}} \mathcal{F}_b \left(\mathcal{F}_a + \frac{\mathcal{F}_b}{6} \right). \quad (92)$$

Note that the second term, proportional to \mathcal{F}_b^2 , coincides with the one-loop QCD correction to the light quark contribution to the $H \rightarrow \gamma\gamma$ decay amplitude presented in [4], see also [39].

For the case when the hard process is $\gamma q \rightarrow qg$ the relevant soft gluon insertions are shown in the diagrams of Fig. 10. Their individual contributions are given in Appendix B. The total result is

$$M_{2\text{-loop}}^{\text{Fig.10}} = M_{\text{Born}} \mathcal{F}_c \left(\mathcal{F}_a + \frac{C_A}{2C_F} \frac{\mathcal{F}_c}{6} \right). \quad (93)$$

The contributions from the $\gamma\bar{q} \rightarrow \bar{q}g$ hard process give the same result, when we take into account (56).

In summary, the complete two-loop correction to the matrix element of the basic process is given by the sum of (91), (92) and twice (93). Using (48) and (55) we have

$$M_{2\text{-loop}} = M_{\text{Born}} \left[\mathcal{F}_a \left(\frac{\mathcal{F}_a}{2} + 3\mathcal{F} \right) + \left(1 + \frac{C_A}{C_F} \right) \frac{\mathcal{F}^2}{6} \right]. \quad (94)$$

Recall that the two-loop contribution $d\sigma_{2\text{-loop}}(\gamma\gamma \rightarrow q\bar{q})$ is the sum of two pieces, namely the sum of (89) and

$$d\sigma_{2\text{-loop}}^{(2)}(\gamma\gamma \rightarrow q\bar{q}) = 2\text{Re}(M_{\text{Born}}^* M_{2\text{-loop}}). \quad (95)$$

Thus we have in total

$$d\sigma_{2\text{-loop}}(\gamma\gamma \rightarrow q\bar{q}) = d\sigma_{\text{Born}}(J_z = 0) \left[2\mathcal{F}_a(\mathcal{F}_a + 6\mathcal{F}) + \mathcal{F}^2 \left(9 + \frac{1}{3} \left(1 + \frac{C_A}{C_F} \right) \right) \right], \quad (96)$$

where \mathcal{F}_a is given by (44) and \mathcal{F} by (48).

5.4 The non-Sudakov form factor F_q

The above results allow us to obtain the two-loop contribution to the non-Sudakov form factor F_q . We substitute (88) and (96) into (72), and use the representation

$$d\sigma_{2\text{-loop}} = d\sigma_{\text{Born}}(J_z = 0) (F_g F_q)_2, \quad (97)$$

where the subscript 2 indicates that we should take the α_s^2 terms in the expansion of the product of the two form factors (F_g is given by (63), and the one-loop approximation to F_q is given in (64)). In this way we obtain

$$\begin{aligned} F_q &= 1 + 6\mathcal{F} + \mathcal{F}^2 \left(9 + \frac{1}{3} \left(1 + \frac{C_A}{C_F} \right) \right) \\ &= (1 + 3\mathcal{F})^2 + \frac{\mathcal{F}^2}{3} \left(1 + \frac{C_A}{C_F} \right). \end{aligned} \quad (98)$$

6. Summary and discussion

We have studied Higgs production in polarised $\gamma\gamma$ collisions. In particular we have investigated the feasibility of the proposal that the Higgs may be isolated in the $\gamma\gamma (J_z = 0) \rightarrow b\bar{b}$ channel, due to the remarkable m_q^2/s suppression of the background process $\gamma\gamma \rightarrow q\bar{q}$. However, the especially large radiative corrections to the background process cause the situation to be much more complicated than it appears at first sight. Indeed it is essential to perform a detailed analysis of the various (real and virtual) background processes since these can greatly exceed the leading order (Born) $\gamma\gamma \rightarrow q\bar{q}$ result.

The general structure of the background arising from the central production of quasi-two-jet-like events with at least one tagged energetic b jet was written in the form

$$\sigma(\gamma\gamma \rightarrow 2\text{jets}) = \sigma(\gamma\gamma \rightarrow q\bar{q})F_g F_q + \sigma(\gamma\gamma \rightarrow q\bar{q}g \rightarrow 2\text{jets})_{\text{collinear+Compton}} \quad (99)$$

see (20). Here it is to be understood that the incoming $\gamma\gamma$ system is in the $J_z = 0$ state. A major problem is that radiative $q\bar{q}g$ production in the collinear and Compton configurations do not have the m_q^2/s suppression, and so could exceed the Born estimate of the background. In the Compton configuration we are concerned with the production of a comparatively soft q or \bar{q} which goes undetected along the beam direction. The contribution was calculated in Section 3 and was found to be quite sizeable, see eqs. (33) - (35). Therefore it should be avoided, if at all possible, by tagging both the energetic b and \bar{b} jets.

Collinear gluon bremsstrahlung off one of quarks was investigated in [18]. It can be suppressed by using traditional cuts to discriminate between the two and three jet topologies, but then due to the Sudakov form factor F_g we also deplete the signal. The Sudakov form factor F_g was given in (66), (68) and (71) for three different cut-off prescriptions.

One of our main aims has been the calculation of the non-Sudakov form factor F_q . It involves novel double logarithmic (DL) terms. Our result, in the two-loop approximation, is shown in (98). Let us summarize the structure of this form factor.

In the one-loop approximation F_q is given by (64). The crucial observation is that the coefficient c_1 in the expansion (21) of F_q in powers of $(\alpha_S/\pi)L_m^2$ is anomalously large and negative, $c_1 = -8$. Thus the cross section, calculated to order α_S accuracy, could formally become negative [21]. At first sight this indicates that it is necessary to sum the whole series. Fortunately we find that it is not the case. The calculation of F_q in the two-loop approximation (98) is quite sufficient, and shows that the higher order coefficients are not so anomalously large. Moreover the large size of c_1 has a simple physical explanation. Recall that F_q is specific to the helicity-violating process and arises from the soft quark contributions. It is not connected with soft real gluon emission which, together with the soft gluon virtual contribution, is absorbed in F_g . Now, the soft quark corrections to the matrix element $M_{\lambda\lambda}^{\lambda\lambda}$ of the basic $\gamma\gamma \rightarrow q\bar{q}$ process come from three different kinematical configurations (or, equivalently are connected with three hard subprocesses, see Figs 4(b) - 4(d)). We thus have a factor 3 enhancement of the amplitude and a factor 6 in the cross section. At higher orders the essential point is that the number of hard subprocesses remains the same. Thus there is a loss of a factor 3 in the two-loop correction to the amplitude as compared with that estimated by the square by the first-order correction. Moreover, the higher-order corrections to F_q arise from kinematical regions where there is one soft quark but several soft gluons, which nevertheless have to be harder than the soft quark since otherwise they are absorbed in F_g . This requirement reduces the higher order coefficients. Equation (94) offers a good example of the above effects. Here we have only to consider the term containing \mathcal{F}^2 because the terms involving \mathcal{F}_a are absorbed in \mathcal{F}_g . Roughly speaking in this case we have a factor $(1 + C_A/C_F) \simeq 3$ corresponding to the number of kinematic regions, while the contribution of each region has a coefficient $1/6$ due to the restrictions on the region of integration over the soft gluon.

In summary, we have presented a full study of the important radiative effects accompanying $\gamma\gamma \rightarrow$ two heavy-quark-jets (in the $J_z = 0$ channel). The aim has been to estimate the contributions from the various radiative background processes to the $H \rightarrow$ two b -jet signal. A more quantitative study will require improvements on both the theoretical and the experimental side. On the theoretical front we will need a self consistent analysis of the single logarithmic terms including the effects of the running mass in the background processes and of the evaluation of the running coupling in both the Sudakov and non-Sudakov form factors. One of the most important experimental questions is the efficiency of b -tagging and of the rejection of $c\bar{c}$ events. There are various different estimates of the level of $c\bar{c}$ contamination, see [13, 18, 19]. Another important task is to find the optimal choice of cut-off prescription to define the two-jet configurations. Finally we note that for an intermediate mass Higgs, say $M_H = 100\text{GeV}$, we find,

using (48) with $\alpha_S(M_H) = 0.12$, that $\mathcal{F} \approx -0.5$ (and -0.9) for $b\bar{b}$ (and $c\bar{c}$) production. From (98) we see that this gives a factor of about 3 suppression in the first term in (99) or (20), which qualitatively justifies the expectations of [18]. At the same time, the potential $c\bar{c}$ non-radiative contribution is enhanced by a factor of about 4.

Acknowledgements

We thank J. Campbell, E.W.N. Glover and W.J. Stirling for discussions. We also thank the UK Particle Physics and Astronomy Research Council for financial support. VSF thanks Grey College of the University of Durham for their warm hospitality and the support of the Russian Fund for Basic Research, as well as INTAS grant 95-0311.

Appendix A

Here we derive the formulae for the one-loop corrections to the amplitude for the process $\gamma\gamma \rightarrow q\bar{q}g$ in the cases of the ‘‘hard’’ subprocesses $q\bar{q} \rightarrow q\bar{q}$ and $\gamma q \rightarrow qg$. The corresponding diagrams are shown in Figs. 6,7. Note that some of these diagrams have contributions which are singular when the emitted gluon is collinear with either of the initial photons. Therefore they will not contribute to the cross section (72), because in the Born approximation we only have collinear singularities when the gluon is emitted in the direction of either the outgoing quark or antiquark. Nevertheless it is useful to evaluate them because each diagram separately gives a contribution, which could lead to double logarithmic terms at $\mathcal{O}(\alpha_S^3)$. Moreover we meet novel double logarithmic terms on account of the helicity-violating nature of the basic process.

We start with diagram 6(a). The contribution of this diagram and the diagram 6(\bar{a}), in which the gluon is emitted from the \bar{q} , can be immediately written down, since the soft gluon cannot influence the hard process. We have

$$M_{1\text{-loop}}^{(1)\text{Fig.6a},\bar{a}} = M_{\text{Born}} \mathcal{F}_b g_S \langle t^a \rangle e_\mu(k_g) J^\mu(k_g). \quad (\text{A.1})$$

Diagram 6(b) can be evaluated using standard techniques. We first neglect the momentum k_g of the soft gluon in the numerator of the matrix element. Now recall that the DL contribution comes from the region where the momentum of the quark which emits the gluon is nearly equal to k_1 . Thus we can reduce the numerator to its value without gluon emission multiplied by $2g_S(e(k_g).k_1)$. In this way we obtain a factorized form similar to (47) but with the replacement

$$\mathcal{F}_b \rightarrow \frac{2g_S(e(k_g).k_1)}{-2k_1.k_g} \frac{(C_F - \frac{1}{2}C_A)}{C_F} \langle t^a \rangle \mathcal{F}_{6b}, \quad (\text{A.2})$$

where \mathcal{F}_{6b} only differs from \mathcal{F}_b by the restriction that

$$|k_1.k| \ll k_1.k_g \quad (\text{A.3})$$

on the region of the k integration in (48). This restriction appears because the contribution from outside the region does not have DL behaviour due to the additional propagator in diagram 6(b) as compared to diagram 4(b). We use Sudakov variables defined by

$$k = \beta k_1 + \alpha k_2 + k_\perp \quad (\text{A.4})$$

to evaluate \mathcal{F}_{6b} . Then restriction (A.3) becomes

$$|\alpha| \ll |\alpha_g| \equiv \frac{k_g.k_1}{k_2.k_1} \quad (\text{A.5})$$

and

$$\begin{aligned} \mathcal{F}_{6b} &= -\frac{\alpha_S}{2\pi} C_F \int_0^1 \int_0^1 \frac{d\alpha}{\alpha} \frac{d\beta}{\beta} \theta(\alpha\beta s - m_q^2) \theta\left(\frac{2k_1.k_g}{s} - \alpha\right) \\ &= -\frac{\alpha_S}{4\pi} C_F \ln^2\left(\frac{2k_1.k_g}{m_q^2}\right), \end{aligned} \quad (\text{A.6})$$

where it is assumed that $s \gg 2k_1.k_g \gg m_q^2$.

In a similar way it is easy to see that diagram 6(c) has the form (47) with the replacement

$$\mathcal{F}_b \rightarrow \frac{-2g_S(e(k_g).k_2)}{-2k_g.k_2} \frac{(C_F - \frac{1}{2}C_A)}{C_F} \langle t^a \rangle \mathcal{F}_{6c} \quad (\text{A.7})$$

where

$$\mathcal{F}_{6c} = -\frac{\alpha_S}{4\pi} C_F \ln^2 \left(\frac{2k_2.k_g}{m_q^2} \right), \quad (\text{A.8})$$

with the limitation that $s \gg 2k_2.k_g \gg m_q^2$.

The evaluation of the contribution of Fig. 6(d) is more complicated due to its spin structure. The result is quite novel. Just as in the original ‘elastic’ amplitude with “hard” subprocess $q\bar{q} \rightarrow q\bar{q}$ of diagram 4(b), the numerators of the q and \bar{q} propagators entering the “hard blob” are well approximated by \not{k}_1 and \not{k}_2 . We use for them the representation (45). However, for the quark line between the photon vertices we have to replace m_q by

$$m_q [\not{k}\phi(k_g) + \phi(k_g)(\not{k} + \not{k}_g)] = m_q [2k.e(k_g) + \phi(k_g)\not{k}_g] \quad (\text{A.9})$$

where k is the quark momentum shown in Fig. 6(d). The spin structure of the first term is the same as the ‘elastic’ case, but the second term has to be treated separately. Using (46) we find we have to calculate the spin matrix element

$$\mathcal{S} \equiv \bar{u}^\lambda(k_1) \not{\epsilon}^\lambda(k_1) \phi(k_g) \not{k}_g \not{\epsilon}^\lambda(k_2) v^\lambda(k_2). \quad (\text{A.10})$$

This matrix element is gauge invariant with respect to the gluon, as well as to the photons. We can reduce it to the ‘elastic’ factorized form (47) by decomposing the four vectors $e(k_g)$ and k_g in terms of k_1, k_2, e_1 and e_2 (where $e_i \equiv e^\lambda(k_i)$) which satisfy

$$\begin{aligned} k_1^2 &= k_2^2 = e_1^2 = e_2^2 = 0, \\ k_i.e_j &= 0 \quad \text{for } i, j = 1, 2, \end{aligned}$$

provided that we choose a gauge in which $k_1.e_2 = k_2.e_1 = 0$. After simple Dirac algebra we find

$$\mathcal{S} = \left[\frac{2(e.k_1)(k_g.k_2)}{(k_1.k_2)} + \frac{2(e.e_1)(k.e_2)}{(e_1.e_2)} \right] \bar{u}^\lambda(k_1) \not{\epsilon}^\lambda(k_1) \not{\epsilon}^\lambda(k_2) v^\lambda(k_2), \quad (\text{A.12})$$

which has the original spin structure of (47). We now use representation (38) for the polarisation vectors e_i to rewrite the second term in the square brackets in the form

$$\begin{aligned} \frac{2(e.e_1)(k_g.e_2)}{(e_1.e_2)} &= -(\mathbf{e}.k_g) + i\lambda(\mathbf{e} \times \mathbf{k}_g).\hat{\mathbf{k}}_1 \\ &= \frac{-e.(k_1(k_g.k_2) + k_2(k_g.k_1))}{k_1.k_2} + i\lambda \frac{\varepsilon_{\mu\nu\rho\sigma} k_2^\mu k_1^\nu e^\rho k_g^\sigma}{k_1.k_2} \end{aligned} \quad (\text{A.13})$$

where $\hat{\mathbf{k}}_i$ is a unit 3-vector and where the $\gamma, \gamma, q, \bar{q}$ helicities are all given by λ , and $\varepsilon_{0123} = 1$ etc. Thus the contribution of diagram 6(d) is obtained from (47) with the replacement

$$\mathcal{F}_b \rightarrow 16g_S(C_F - \frac{1}{2}C_A) \langle t^a \rangle \left(\frac{-\alpha_S}{4\pi} \right) I, \quad (\text{A.14})$$

where the integral

$$I = \int \frac{d^4k}{i(2\pi)^2} \frac{e \cdot (2k(k_1 \cdot k_2) + k_1(k_g \cdot k_2) - k_2(k_g \cdot k_1)) + i\lambda \varepsilon_{\mu\nu\rho\sigma} k_2^\mu k_1^\nu e^\rho k_g^\sigma}{[(k+k_1)^2 - m_q^2 + i\varepsilon][(k+k_g-k_2)^2 - m_q^2 + i\varepsilon][(k+k_g)^2 - m_q^2 + i\varepsilon][k^2 - m_q^2 + i\varepsilon]} \quad (\text{A.15})$$

This integral may be evaluated using the Feynman parameter technique. We define x_i to be the Feynman parameter for the i th denominator in the integrand. We perform the exact integration over x_4 and x_3 , and obtain

$$I = \frac{1}{4} \int_0^1 \int_0^1 dx_1 dx_2 (1-x_1-x_2) \theta(1-x_1-x_2) \times \frac{(e \cdot k_1)(k_g \cdot k_2 - 2x_1 k_1 \cdot k_2) - (e \cdot k_2)(k_g \cdot k_1 - 2x_2 k_1 \cdot k_2) + i\lambda \varepsilon_{\mu\nu\rho\sigma} k_2^\mu k_1^\nu e^\rho k_g^\sigma}{D_1 D_2} \quad (\text{A.16})$$

with

$$D_i \equiv -2x_1 x_2 (k_1 \cdot k_2 - k_j \cdot k_g) + 2x_i (1-x_i) k_i \cdot k_g + m_q^2 - i\varepsilon$$

where $k_j = k_1$ if $i = 2$ and $k_j = k_2$ if $i = 1$. We now extract the double logarithmic behaviour from this integral form and find

$$16I = \frac{e \cdot k_1}{k_g \cdot k_1} \ln^2 \left(\frac{2k_g \cdot k_1}{m_q^2} \right) - \frac{e \cdot k_2}{k_g \cdot k_2} \ln^2 \left(\frac{2k_g \cdot k_2}{m_q^2} \right) + i\lambda \frac{\varepsilon_{\mu\nu\rho\sigma} k_2^\mu k_1^\nu e^\rho k_g^\sigma}{(k_g \cdot k_1)(k_g \cdot k_2)} \ln^2 \left(\frac{(k_g \cdot k_1)(k_g \cdot k_2)}{m_q^2 (k_1 \cdot k_2)} \right), \quad (\text{A.17})$$

where it has been assumed that the arguments of all the logarithms are large⁹.

If we now combine together all the contributions coming from the diagrams of Fig. 6 we obtain (80). Note that all terms proportional to $(e \cdot k_i)$ cancel each other.

Now we consider the contribution of the diagrams of Fig. 7, which arise by adding a soft gluon line to diagram 4(c). First, the contribution of diagram 7(a), together with the crossed diagram with $k_1 \leftrightarrow k_2$, has the factorised form

$$M_{1\text{-loop}}^{(1)\text{ Fig.7a}} = M_{\text{Born}} g_S \langle t^a \rangle \frac{e \cdot p}{k_g \cdot p} \mathcal{F}_c. \quad (\text{A.18})$$

⁹More precisely each logarithm is only taken into account when its argument is large. This assumption is made throughout this Appendix.

In a similar way the contribution of diagram 7(b) has the form (58) with the replacement

$$\mathcal{F}_c \rightarrow -g_S \langle t^a \rangle \frac{e \cdot \bar{p}}{k_g \cdot \bar{p}} \mathcal{F}_{7b}, \quad (\text{A.19})$$

but now \mathcal{F}_{7b} is obtained from \mathcal{F}_c with the limitation

$$|k \cdot \bar{p}| \gg k_g \cdot \bar{p} \quad (\text{A.20})$$

on the k integration in (52). Thus we have

$$\mathcal{F}_{7b} = -\frac{\alpha_S}{4\pi} C_F \left[\ln^2 \left(\frac{2k_2 \cdot \bar{p}}{m_q^2} \right) - \ln^2 \left(\frac{2k_g \cdot \bar{p}}{m_q^2} \right) \right], \quad (\text{A.21})$$

where, as always, we assume that the arguments of the logarithms are large.

The contributions of diagrams 7(c,d) can be calculated in a similar way to that used for diagrams 6(b,c). Thus they have the form of (58) with the following replacements respectively

$$\mathcal{F}_c \rightarrow -g_S \langle t^a \rangle (C_F - \frac{1}{2}C_A) \frac{e \cdot k_2}{k_g \cdot k_2} \left(\frac{-\alpha_S}{4\pi} \right) \ln^2 \left(\frac{2k_g \cdot k_2}{m_q^2} \right), \quad (\text{A.22})$$

$$\mathcal{F}_d \rightarrow -g_S \langle t^a \rangle \frac{1}{2}C_A \frac{e \cdot \bar{p}}{k_g \cdot \bar{p}} \left(\frac{-\alpha_S}{4\pi} \right) \ln^2 \left(\frac{2k_g \cdot \bar{p}}{m_q^2} \right). \quad (\text{A.23})$$

Finally diagram 7(e) may be evaluated in a similar way to diagram 6(d). Again its contribution is the form of (58), but now with the replacement

$$\begin{aligned} \mathcal{F}_c \rightarrow & g_S \langle t^a \rangle (C_F - \frac{1}{2}C_A) \left(\frac{-\alpha_S}{4\pi} \right) \left[\frac{e \cdot k_2}{k_g \cdot k_2} \ln^2 \left(\frac{2k_g \cdot k_2}{m_q^2} \right) \right. \\ & \left. - \frac{e \cdot \bar{p}}{k_g \cdot \bar{p}} \ln^2 \left(\frac{2k_g \cdot \bar{p}}{m_q^2} \right) + i\lambda \frac{\varepsilon_{\mu\nu\rho\sigma} \bar{p}^\mu k_2^\nu e^\rho k_g^\sigma}{(k_g \cdot k_2)(k_g \cdot \bar{p})} \ln^2 \left(\frac{(k_g \cdot \bar{p})(k_g \cdot k_2)}{m_q^2 (k_2 \cdot \bar{p})} \right) \right]. \end{aligned} \quad (\text{A.24})$$

Combining together all the above contributions of Fig. 7 we finally obtain (82). We see the cancellations of the spurious $k_g \cdot k_1$ and $k_g \cdot k_2$ singularities. These singularities in the $\varepsilon_{\mu\nu\rho\sigma}$ term cancel in the total $M_{1\text{-loop}}^{(1)}$ contribution given in (86).

Appendix B

Here we derive the DL corrections, (92) and (93), connected with the hard processes $q\bar{q} \rightarrow q\bar{q}$ and $\gamma q \rightarrow gq$ respectively. The diagrams for the first case are shown in Fig. 9. The contribution of diagram 9(a) can be written down immediately. The exchange of the soft quark with momentum k_q occurs before, whereas the exchange of soft gluon with momentum k_g occurs after, the hard $q\bar{q} \rightarrow q\bar{q}$ scattering. Thus, since the exchanges do not influence each other, we have

$$M^{\text{Fig.9a}} = M_{\text{Born}} \mathcal{F}_a \mathcal{F}_b. \quad (\text{B.1})$$

Recall that this amplitude (and those below) represents the sum of the contribution of diagram 9(a) and the diagram with the photon momenta interchanged.

For the calculation of the contribution of diagram 9(b) it is convenient to use the Sudakov decomposition of the momenta of the soft particles

$$k_i = \beta_i k_1 + \alpha_i k_2 + k_{iT}, \quad (\text{B.2})$$

where $i = (\text{soft}) q$ or g . Recall that the DL contributions come from the regions

$$1 \gg |\alpha_i|, |\beta_i| \gg |k_{iT}^2/s| \gg |m_i^2/s| \quad (\text{B.3})$$

and can be calculated performing the integration over the corresponding transverse momenta of the soft particles by taking half of the residues in the corresponding propagators

$$\begin{aligned} \frac{d^4 k_i}{k_i^2 - m_i^2 + i\varepsilon} &= \left(\frac{s}{2}\right) \frac{d\alpha_i d\beta_i d^2 k_{iT}}{s\alpha_i\beta_i - \mathbf{k}_{iT}^2 - m_i^2 + i\varepsilon} \\ &\rightarrow -i\pi^2 \left(\frac{s}{2}\right) d\alpha_i d\beta_i \Theta(s\alpha_i\beta_i - m_i^2). \end{aligned} \quad (\text{B.4})$$

Thus the DL contribution has the form

$$M_i = M_{\text{Born}} \mathcal{F}_i, \quad (\text{B.5})$$

where \mathcal{F}_i are given by integrals over α_i and β_i

$$\begin{aligned} \mathcal{F}_i &= \left(\frac{\alpha_S}{2\pi}\right)^2 \int_0^1 \int_0^1 \frac{d\alpha_q}{\alpha_q} \frac{d\beta_q}{\beta_q} \Theta\left(\alpha_q\beta_q - \frac{m_q^2}{s}\right) \\ &\quad \times \int_0^1 \int_0^1 \frac{d\alpha_g}{\alpha_g} \frac{d\beta_g}{\beta_g} \Theta\left(\alpha_g\beta_g - \frac{m_g^2}{s}\right) C_i, \end{aligned} \quad (\text{B.6})$$

The factor C_i includes both the appropriate colour factors and the restrictions on α_i and β_i necessary to ensure that the matrix element has logarithmic behaviour in each of the variables α_i and β_i . For the contribution of diagram 9(b) we find

$$C_{9b} = C_F^2 \Theta(\alpha_g - \alpha_q) \Theta(\beta_g - \beta_q), \quad (\text{B.7})$$

and therefore we obtain

$$\mathcal{F}_{9b} = \frac{1}{6} \mathcal{F}^2, \quad (\text{B.8})$$

where from (48) we have

$$\mathcal{F} = -\frac{\alpha_S}{\pi} C_F \ln^2 \left(\frac{M_H}{m_q} \right). \quad (\text{B.9})$$

The DL contributions of the other diagrams can be calculated in a similar way, provided that we use an appropriate choice of the base vectors of the Sudakov decomposition. For the soft quark the choice is the same for all the diagrams of Fig. 9. However, for the soft gluon it is convenient to use the light cone momenta k_1 and $(p - m_q^2 k_1 / 2p \cdot k_1)$ for diagram 9(c), k_2 and $(\bar{p} - m_q^2 k_2 / 2\bar{p} \cdot k_2)$ for diagram 9(d), and so on. Since we consider large angle $q\bar{q}$ production, we have

$$2p \cdot k_1 = 2\bar{p} \cdot k_2 \sim 2p \cdot k_2 = 2\bar{p} \cdot k_1 \sim 2p \cdot \bar{p} \sim 2k_1 \cdot k_2 = s \quad (\text{B.10})$$

and therefore we can neglect the difference between these variables in the arguments of the logarithms. Thus for diagrams 9(c) - 9(f) the factors C_i of (B.6) can be shown to be

$$\begin{aligned} C_{9c} &= -C_{9e} = C_F \left(C_F - \frac{C_A}{2} \right) \Theta(\alpha_g - \alpha_q) \Theta \left(\beta_g - \frac{m_q^2}{s} \alpha_g \right); \\ C_{9d} &= -C_{9f} = C_F \left(C_F - \frac{C_A}{2} \right) \Theta(\beta_g - \beta_q) \Theta \left(\alpha_g - \frac{m_q^2}{s} \beta_g \right); \end{aligned} \quad (\text{B.11})$$

so the DL contributions of these diagrams cancel each other.

It is also evident that the DL contributions of diagrams 9(g) and 9(h) will cancel each other, just as, for example, the contributions of 9(c) and 9(e) cancel each other. In fact a simple observation shows that 9(g) and 9(h) are individually zero in the DL approximation. Indeed, if we perform an integration over the soft quark momentum for a fixed value of the momentum of the soft gluon then we see that the result is antisymmetric with respect to the replacement $k_1 \leftrightarrow k_2$, just as in the real emission case, see (A.6). Since the large variables (B.10) in the DL factors do not differ we conclude the contributions of diagrams 9(g) and 9(h) are separately zero. Thus we are left with the sum of diagrams 9(a) and 9(b), that is of (B.1) and (B.8), which gives the result stated in (92).

We now turn to the diagrams shown in Fig. 10. Their DL contributions can be calculated in a similar way. We give below the results for the C_i factors occurring in representation (B.5), (B.6) for the individual diagrams

$$\begin{aligned} C_{10a} &= C_F^2 \Theta \left(\alpha_g - \frac{m_q^2}{s} \beta_g \right) \Theta \left(\beta_g - \frac{m_q^2}{s} \alpha_g \right) \Theta(\beta_q - \beta_g); \\ C_{10b} &= C_F \left(C_F - \frac{C_A}{2} \right) \Theta(\alpha_q - \alpha_g) \Theta(\beta_g - \beta_q) \Theta \left(\alpha_g - \frac{m_q^2}{s} \beta_g \right); \end{aligned}$$

$$\begin{aligned}
C_{10c} &= C_F \frac{C_A}{2} \Theta(\beta_g - \beta_q) \Theta\left(\alpha_g - \frac{m_q^2}{s} \beta_g\right); \\
C_{10d} &= C_F \left(C_F - \frac{C_A}{2}\right) \Theta(\beta_g - \beta_q) \Theta\left(\alpha_g - \frac{m_q^2}{s} \beta_g\right); \\
C_{10e} &= -C_F \left(C_F - \frac{C_A}{2}\right) \Theta(\beta_g - \beta_q) \Theta(\alpha_q - \alpha_g) \Theta\left(\alpha_g - \frac{m_q^2}{s} \beta_g\right); \\
C_{10f} &= C_F \frac{C_A}{2} \Theta(\alpha_g - \alpha_q) \Theta(\beta_g - \beta_q); \\
C_{10g} &= 0.
\end{aligned} \tag{B.12}$$

Using these results it is straightforward to show that the total DL contribution of Fig. 10 is given by (93).

References

- [1] J.F. Gunion, H.E. Haber, G. Kane and S. Dawson, *The Higgs hunter's guide* (Addison-Wesley Reading, MA, 1990).
- [2] S. Dawson, *Perspectives on Higgs Physics*, ed. G. Kane, World Scientific Publ. (1992), p. 129;
J.F. Gunion, *ibid.*, p. 179;
Z. Kunszt, *ibid.*, p. 156.
- [3] B.A. Kniehl, *Phys. Rep.* **240** (1994) 211; *Int. J. Mod. Phys.* **A10** (1995) 443.
- [4] M. Spira, A. Djouadi, D. Graudenz and P.M. Zerwas, *Nucl. Phys.* **B453** (1995) 17.
- [5] A. Djouadi *et al.*, *Higgs Particles* (The European Working Groups on Physics with e^+e^- Linear Colliders), Karlsruhe preprint KA-TP-16-96.
- [6] M. Carena, P.M. Zerwas, E. Accomando *et al.*, *Higgs physics*, in *Physics at LEP2*, CERN 96-01, vol. 1, p. 351.
- [7] G. Bélanger, in *Photon '95*, eds. D.J. Miller, S.L. Cartwright and V. Khoze, World Scientific Publ. (1995), p. 381.
- [8] I.F. Ginzburg, *ibid*, p. 399.
- [9] V.A. Khoze, *ibid*, p. 392.
- [10] I.F. Ginzburg *et al.*, *Nucl. Inst. Meth.* **205**, 47 (1983); *ibid*, **219**, 5 (1984).
- [11] V.I. Telnov, *Nucl. Inst. Meth.* **A355** (1995) 3; in *Photon '95*, eds. D.J. Miller, S.L. Cartwright and V. Khoze, World Scientific Publ. (1995), p. 369.
- [12] J.F. Gunion and H.E. Haber, *Phys. Rev.* **D48**, 5109 (1993).
- [13] D.L. Borden, D.A. Bauer and D.O. Caldwell, preprint UCSB-HEP-92-01 (1992); *Phys. Rev.* **D48** (1993) 4018.
- [14] J. Ellis, M.K. Gaillard and D.V. Nanopoulos, *Nucl. Phys.* **B106** (1976) 292.
- [15] B.L. Ioffe and V.A. Khoze, Leningrad preprint LNPI-274 (1976), *Sov. J. Part. Nucl.* **9** (1978) 50.
- [16] K.A. Ispiryan, I.A. Nagorskaya, A.G. Oganesyanyan and V.A. Khoze, *Sov. J. Nucl. Phys.* **11**, 712 (1970).
- [17] T. Barklow, SLAC preprint, SLAC-PUB-5364 (1990).
- [18] D.L. Borden, V.A. Khoze, W.J. Stirling and J. Ohnemus, *Phys. Rev.* **D50** (1994) 4499.

- [19] T. Ohgaki, T. Takahashi and I. Watanabe, Hiroshima University preprint, HUPD-9705, March 1997.
- [20] M. Baillargeon, G. Bélanger and F. Boudjema, *Phys. Rev.* **D51** (1995) 4712.
- [21] G. Jikia and A. Tkabladze, *Phys. Rev.* **D54** (1996) 2030.
- [22] G. Jikia and A. Tkabladze, *Nucl. Inst. Meth.* **A355** (1995) 81.
- [23] B. Kamal, Z. Merebashvili and A.P. Contogouris, *Phys. Rev.* **D51** (1995) 4808.
- [24] V.V. Sudakov, *Sov. Phys. JETP* **3** (1956) 65.
- [25] E. Braaten and J.P. Leveille, *Phys. Rev.* **D22** (1980) 715;
M. Drees and K.I. Hikasa, *Phys. Lett.* **B240** (1990) 455; *Phys. Rev.* **D41** (1990) 1547.
- [26] R. Kleiss, Z. Kunszt and W.J. Stirling, *Phys. Lett.* **B253** (1991) 269.
- [27] A.L. Kataev and V.T. Kim, *Mod. Phys. Lett.* **A9** (1994) 1309.
- [28] W.A. Bardeen, A.J. Buras, D.W. Duke and T. Muta, *Phys. Rev.* **D18** (1978) 3998.
- [29] V.N. Baier, V.S. Fadin and V.A. Khoze, *Nucl. Phys.* **B65** (1973) 381.
- [30] F.W. Lipps and H.A. Tolhoek, *Physica* **20** (1954) 395;
W.H. McMaster, *Rev. Mod. Phys.* **33** (1961) 8;
V.P. Gavrilov, I.A. Nagorskaya and V.A. Khoze, *Izvestiya AN Armenian SSR, Fizika* **4** (1969) 137.
- [31] V.B. Berestetskii, E.M. Lifshitz and L.P. Pitaevskii, *Quantum Electrodynamics*, Pergamon Press, Oxford (1982).
- [32] V.G. Gorshkov, *Sov. Phys., Uspekhi*, **16** (1973) 322.
- [33] J. Collins, in *Perturbative QCD*, ed. A.H. Mueller, p.573, World Scientific, Singapore 1989.
- [34] V.G. Gorshkov, V.N. Gribov, L.N. Lipatov and G.V. Frolov, *Sov. J. Nucl. Phys.* **6** (1967) 95.
- [35] R. Kirschner and L.N. Lipatov, *Nucl. Phys.* **B213** (1983) 122.
- [36] J. Bartels, B.I. Ermolaev and M.G. Ryskin, *Z. Phys.* **C70** (1996) 273; *Z. Phys.* **C72** (1996) 627;
B.I. Ermolaev, S.I. Manayenkov and M.G. Ryskin, *Z. Phys.* **C69** (1996) 259.
- [37] A.I. Vainstein, M.B. Voloshin, V.I. Zakharov and M.A. Shifman, *Sov. J. Nucl. Phys* **30** (1979) 711.

[38] E.A. Kuraev and V.S. Fadin, *Sov. J. Nucl. Phys.* **27** (1978) 587.

[39] M. Kotsky and O. Yakovlev, to be published

Figure Captions

- Fig. 1 A virtual contribution to the background process $\gamma\gamma \rightarrow q\bar{q}$. There is also a contribution with $k_1 \leftrightarrow k_2$. These are the only one-loop diagrams which give non-vanishing contributions in the $m_q = 0$ limit if the helicities of the photons are equal.
- Fig. 2 The Compton configuration of $\gamma\gamma \rightarrow q\bar{q}g$ which can fake the Higgs signal if only one energetic b jet is tagged. There are also contributions with $q \leftrightarrow \bar{q}$ and/or $k_1 \leftrightarrow k_2$.
- Fig. 3 The diagram which gives a DL contribution to backward electron-muon scattering.
- Fig. 4 Four (non-overlapping) configurations which give $\mathcal{O}(\alpha_S)$ DL corrections to $\gamma\gamma \rightarrow q\bar{q}$. For diagrams (b), (c) and (d) there are also contributions with $k_1 \leftrightarrow k_2$.
- Fig. 5 The soft gluon emissions in the case when the hard subprocess is $\gamma\gamma \rightarrow q\bar{q}$. We also have diagrams (labelled $5(\bar{a}, \bar{b}, \bar{d})$ in the text) in which the gluon is emitted from the \bar{q} rather than the q . In addition all these diagrams have counterparts with $k_1 \leftrightarrow k_2$.
- Fig. 6 The soft gluon emission from the diagram shown in Fig. 4(b). There is also a diagram (labelled $6(\bar{a})$ in the text) where the gluon is emitted from the \bar{q} rather than the q . In addition all these diagrams have counterparts with $k_1 \leftrightarrow k_2$.
- Fig. 7 The soft gluon emission from the diagram shown in Fig. 4(c). There are also contributions with $k_1 \leftrightarrow k_2$.
- Fig. 8 Diagrams for the non-radiative 2-loop corrections when the hard subprocess is $\gamma\gamma \rightarrow q\bar{q}$.
- Fig. 9 Diagrams for the non-radiative 2-loop corrections when the hard subprocess is $q\bar{q} \rightarrow q\bar{q}$. There are also contributions with $k_1 \leftrightarrow k_2$.
- Fig. 10 Diagrams for the non-radiative 2-loop corrections when the hard subprocess is $\gamma q \rightarrow qg$. There are also contributions with $k_1 \leftrightarrow k_2$.

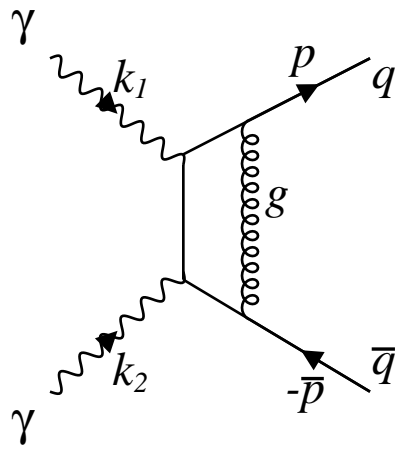


Fig.1

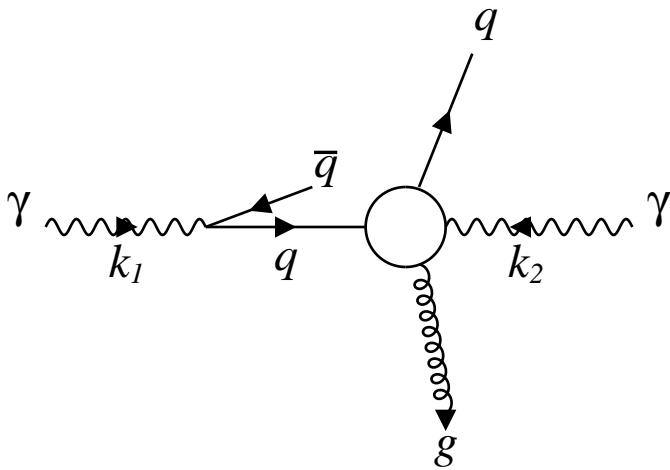


Fig.2

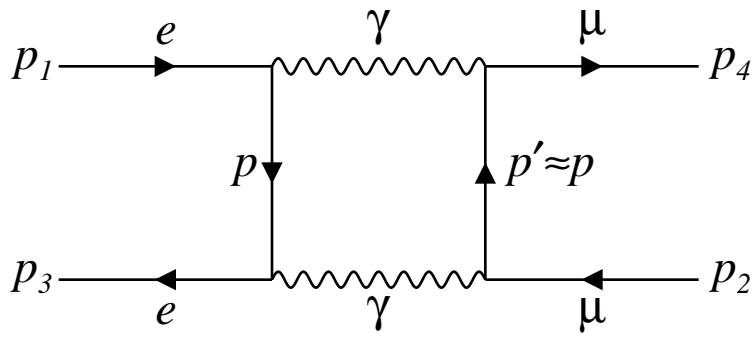


Fig.3

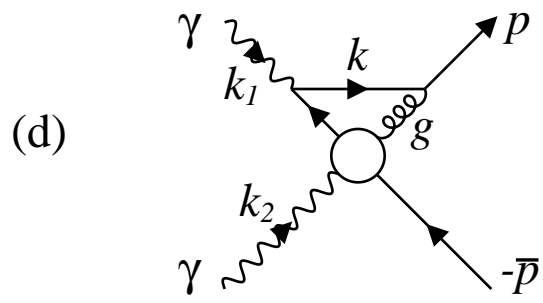
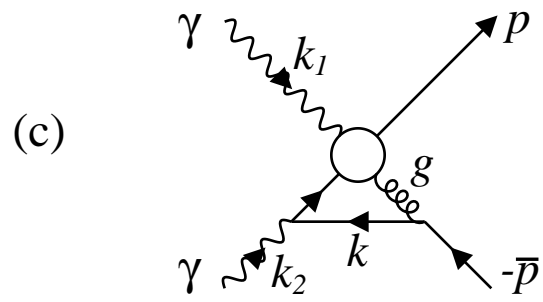
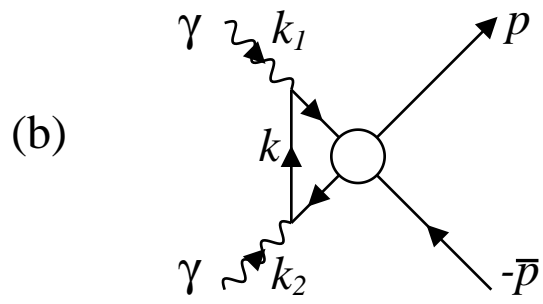
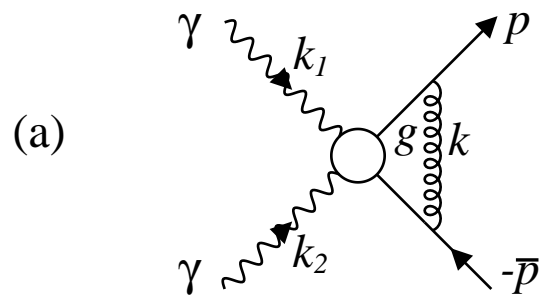


Fig.4

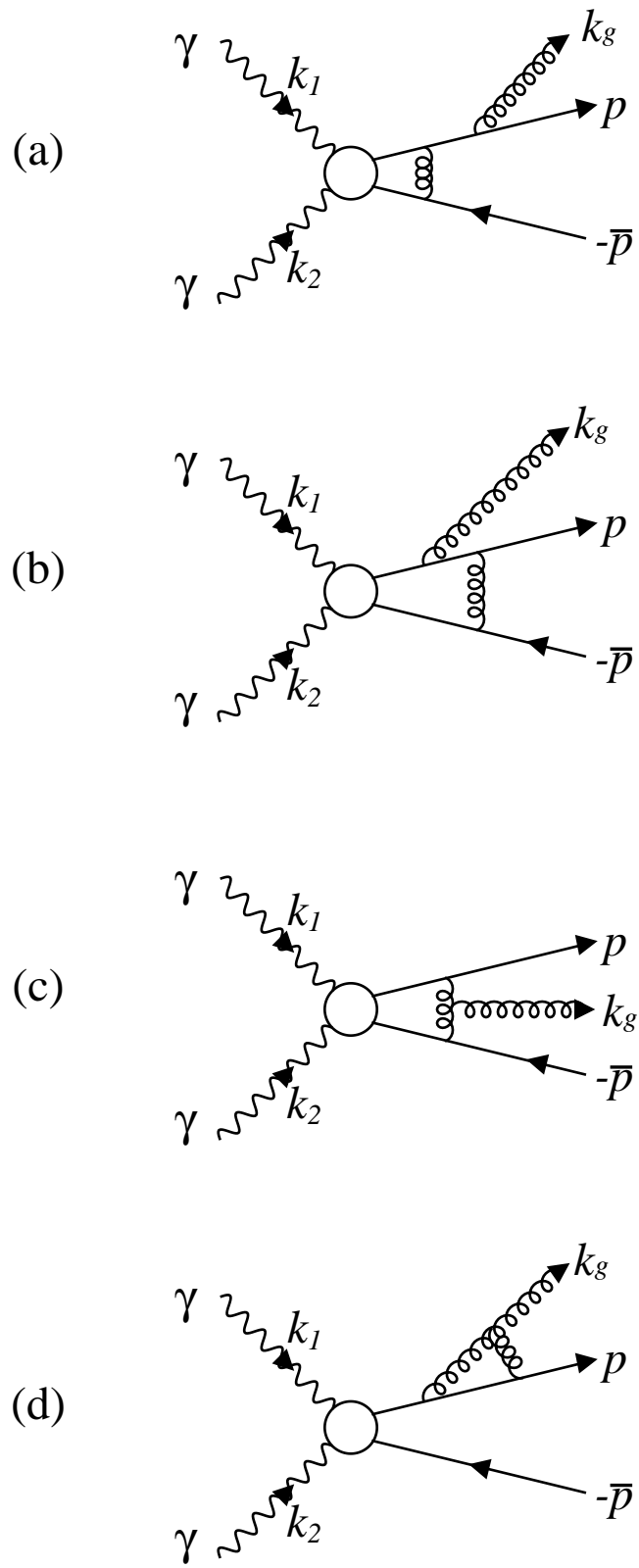


Fig.5

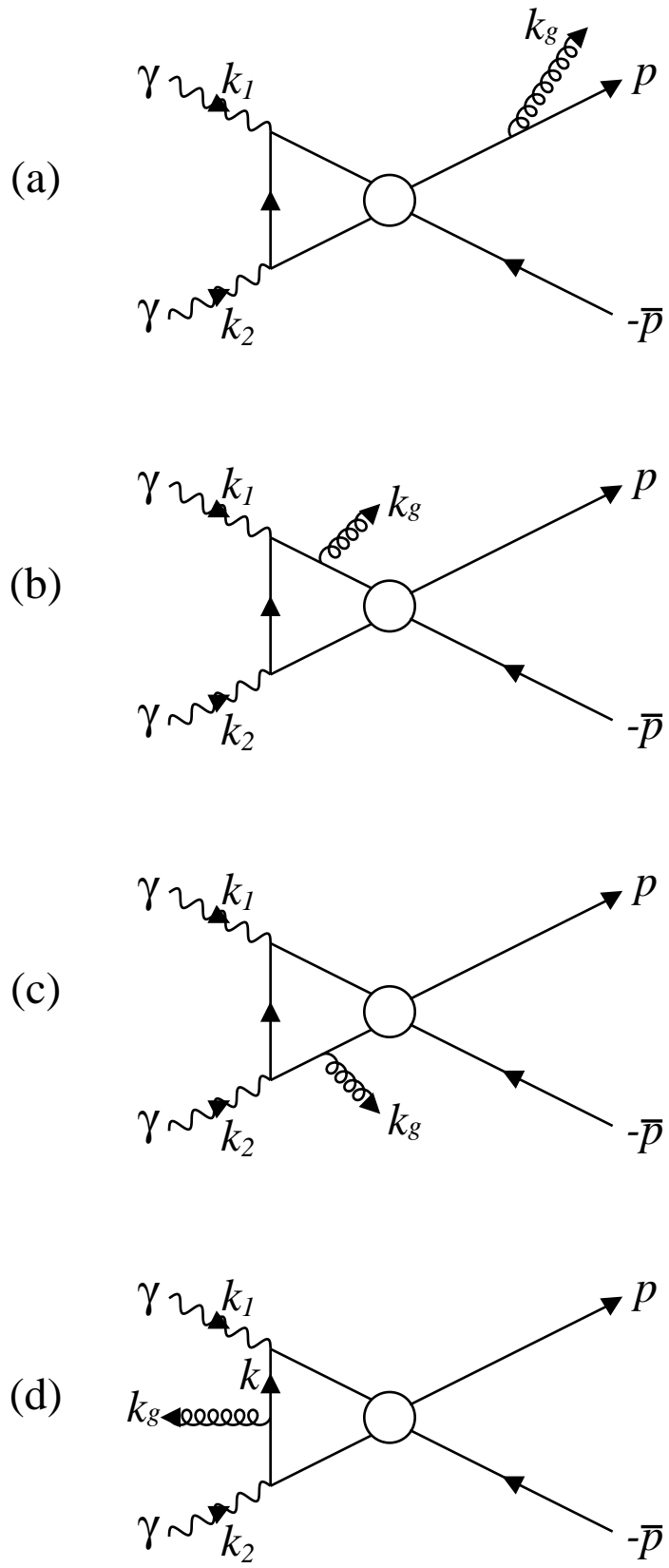


Fig.6

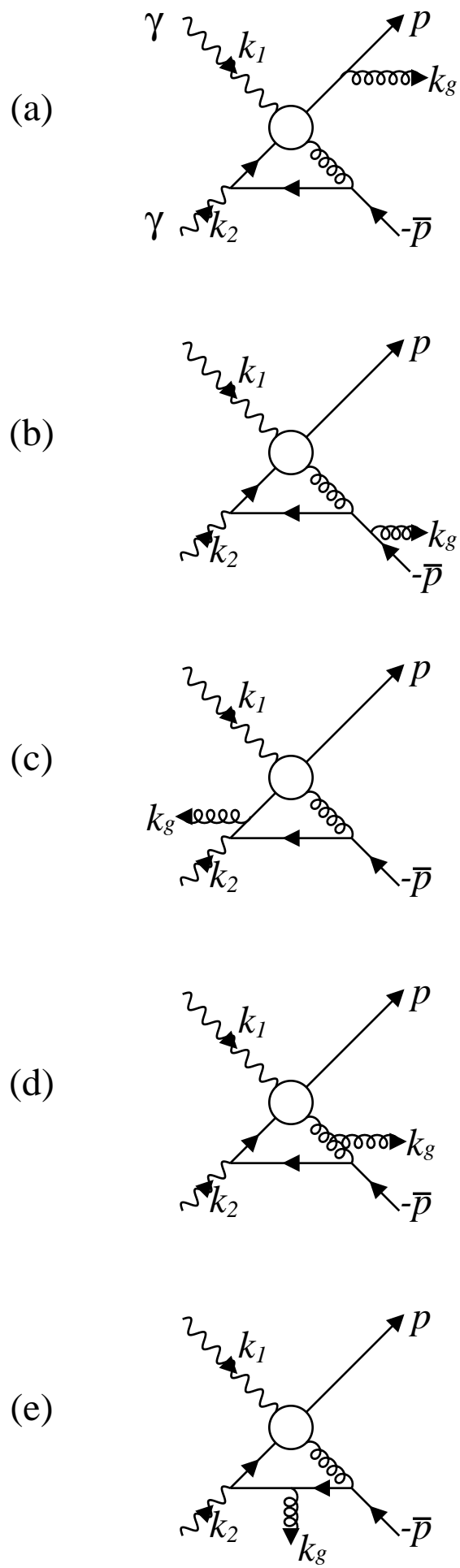


Fig.7

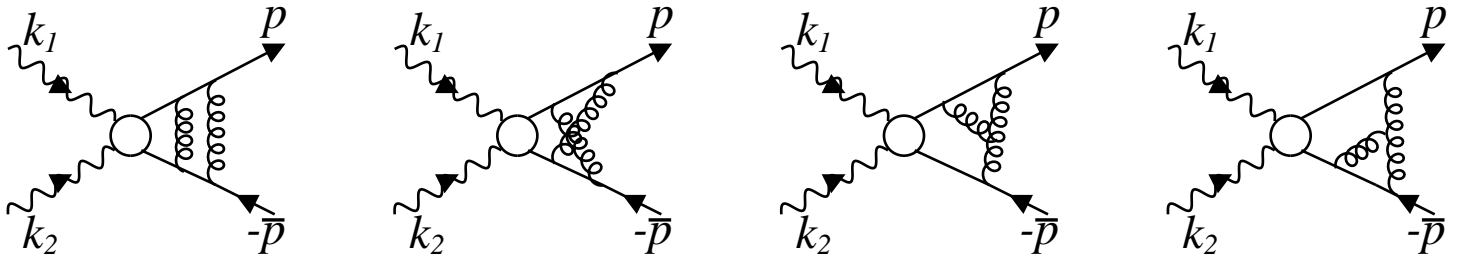


Fig.8

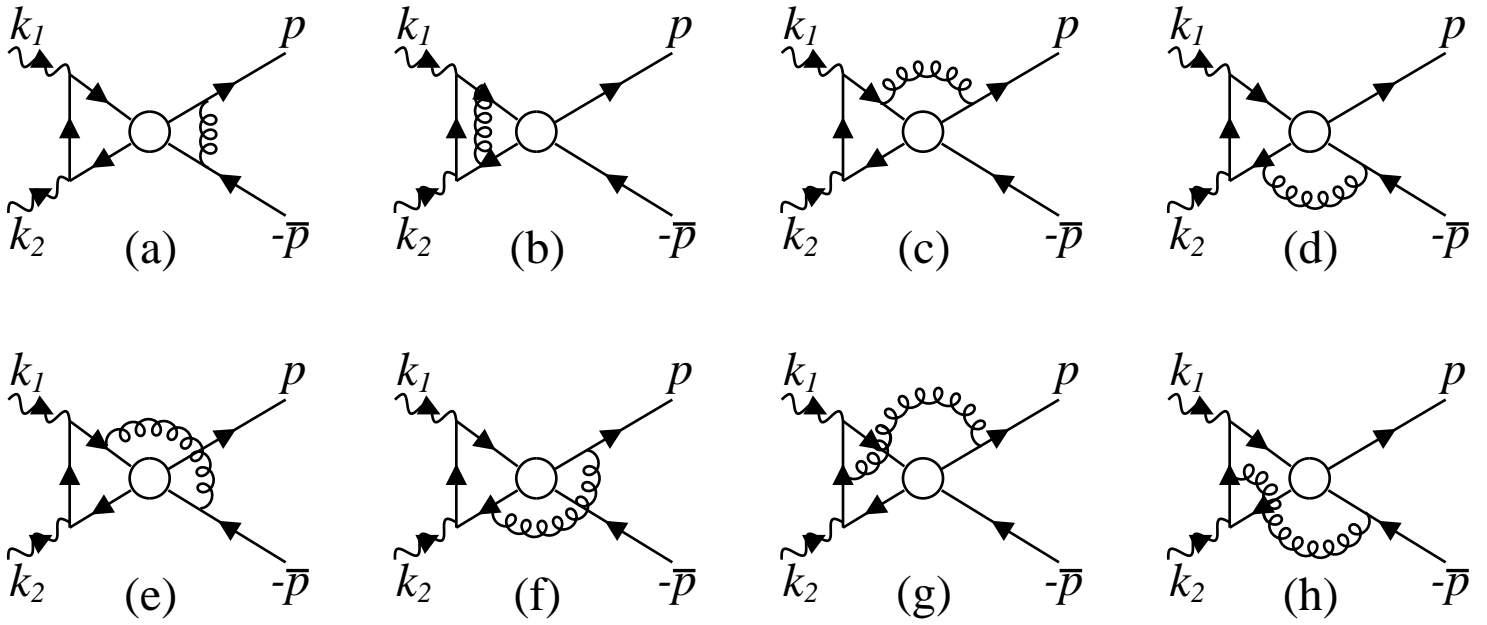


Fig.9

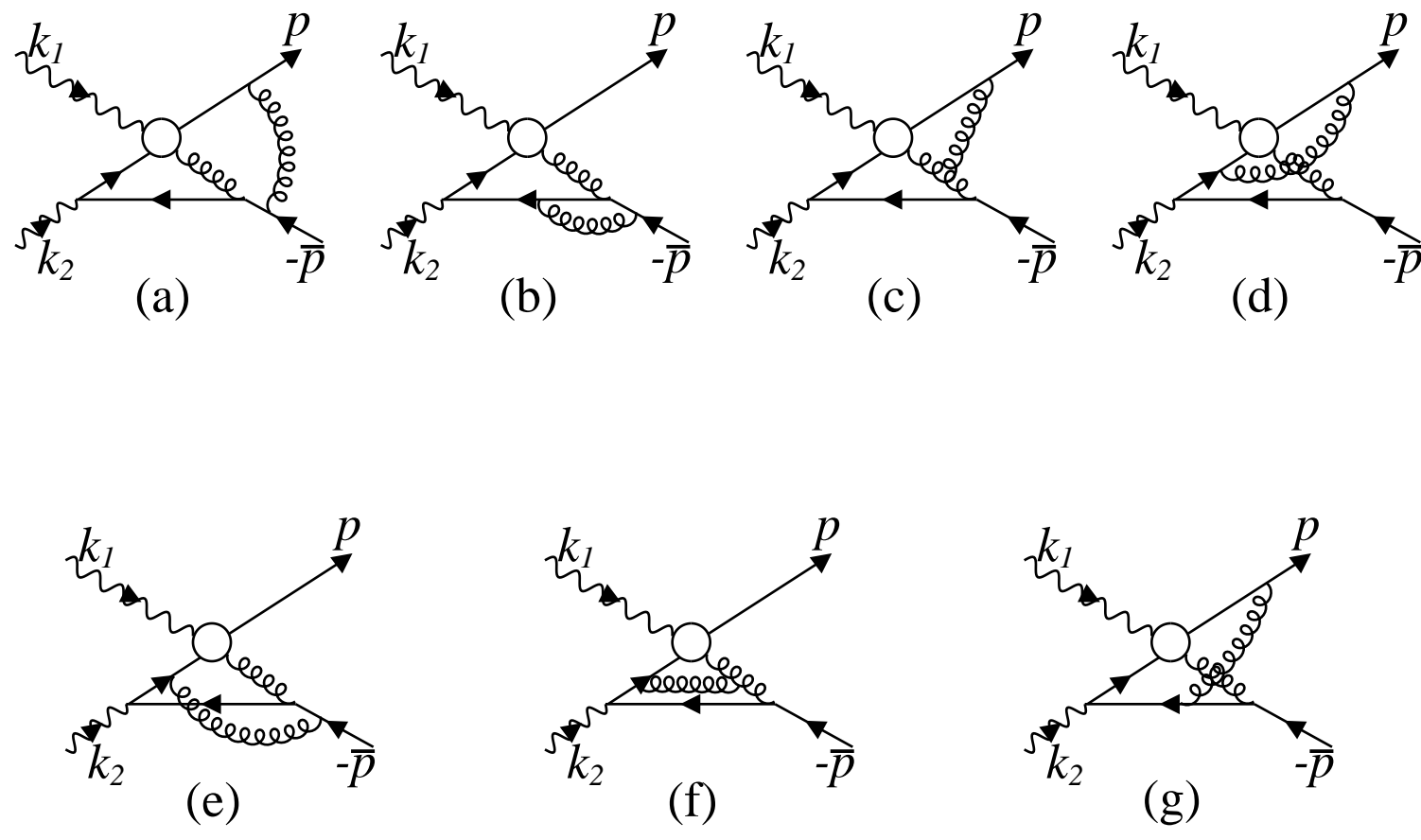


Fig.10